$\cos 2\phi_t$ azimuthal asymmetry in back-to-back J/ψ-jet production in $ep \to eJ/\psi$ jet X at the EIC

Raj Kishore,[1,*] Asmita Mukherjee,[2,†] Amol Pawar,[2,‡] and Mariyah Siddiqah[2,§]

[1]*Department of Physics, Indian Institute of Technology Kanpur, Kanpur-208016, India*
[2]*Department of Physics, Indian Institute of Technology Bombay, Mumbai-400076, India*

(Received 4 April 2022; accepted 20 July 2022; published 10 August 2022)

In this article, we investigate the $\cos 2\phi_t$ azimuthal asymmetry in $ep \to eJ/\psi$ jet X, where the J/ψ-jet pair is almost back to back in the transverse plane, within the framework of the generalized parton model. We use nonrelativistic QCD (NRQCD) to calculate the J/ψ production amplitude and incorporate both color singlet and color octet contributions to the asymmetry. We estimate the asymmetry using different parametrizations of the gluon transverse-momentum-dependent parton distributions in the kinematics that can be accessed at the future electron-ion collider (EIC) and also investigate the impact of transverse-momentum-dependent evolution on the asymmetry. We present the contributions coming from different states to the asymmetry in NRQCD.

DOI: 10.1103/PhysRevD.106.034009

I. INTRODUCTION

Transverse-momentum-dependent parton distributions (TMDs) [1–6] give a tomographic picture of the nucleon in terms of quarks and gluons in momentum space. TMDs play an important role in processes where two scales are involved—for example, in semi-inclusive deep inelastic scattering (SIDIS), where, apart from the photon virtuality, one measures the transverse momentum of the outgoing particle, or a Drell-Yan (DY) process, where the transverse momentum of the outgoing lepton pair provides the second scale. For such processes, one can apply the generalized factorization involving TMDs. However, the TMD factorization has not been proven for all processes. In the kinematical limit when the collinear factorization becomes valid, the result based on TMD factorization should be matched with that obtained using collinear factorization in the same process, with the inclusion of soft factors in the TMD framework [7–12]. To ensure gauge invariance, the TMDs include gauge links or Wilson lines, which come due to initial or final state interactions [13–16]. These introduce process dependence in them. Recent results from RHIC are in favor of the theoretical prediction of a sign change of the Sivers function observed in SIDIS and DY processes, respectively [17]. More data are needed to have a firm understanding of the process dependence of the TMDs. Gluon TMDs [18] till now are far less investigated than quark TMDs. The positivity bound gives a constraint on them [18]. Recently, there was an extraction of unpolarized gluon TMDs from LHCb data [19]. Gauge invariance of the gluon TMDs requires the inclusion of two gauge links in the definition, which makes the process dependence more involved than the quark TMDs [20]. The most common are one past- and one future-pointing gauge link, $[+-]$ or $[-+]$ (f-type), and both past or both future pointing, $[--]$ or $[++]$ (d-type). The operator structures of these two types of gluon TMDs are different [20]. In the literature on small-x physics, these two gluon TMDs are called Weizsacker-Williams (WW) [21,22] type and dipole [23] type, respectively. These contribute in different processes.

In an unpolarized proton, there is a nonzero probability of finding linearly polarized gluons. The linearly polarized gluon distributions were introduced in Ref. [18] and first investigated in a model in Ref. [24]. Recently, these have attracted quite a lot of attention, although till now they have not been extracted using data. Linearly polarized gluon distributions can be probed in ep and pp collisions [25–38]. These give an azimuthal asymmetry of the form $\cos 2\phi_t$ [26]; also, they affect the transverse momentum distribution of the outgoing particle. Depending on the gauge links, the linearly polarized gluon distribution can be WW or dipole type. These are time reversal even (T-even) objects. In pp scattering processes, the initial and final state interactions often affect the TMD factorization; the asymmetries and cross sections also involve both f-type and

*raj.theps@gmail.com
†asmita@phy.iitb.ac.in
‡194120018@iitb.ac.in
§shah.siddiqah@gmail.com

d-type gluon TMDs, and disentangling the two is difficult from the observables. The gauge link structure is simpler in ep scattering processes [39], and the upcoming electron-ion collider (EIC) at Brookhaven National Lab will play an important role in probing the gluon TMDs, including the linearly polarized gluon TMD over a wide kinematical region.

$\cos 2\phi_t$ asymmetry in J/ψ production in unpolarized ep collision has been shown to be a useful observable to probe the linearly polarized gluon TMD. Contribution to the asymmetry comes already at the leading order (LO) through the virtual photon-gluon fusion process [40]; this contributes at $z = 1$, where z is the fraction of the energy of the photon carried by the J/ψ in the rest frame of the proton. In the kinematical region $z < 1$ [41], one has to incorporate higher-order Feynman diagrams. In this process, the J/ψ produced needs to be detected in the forward region or with its transverse momentum p_T not so large; otherwise, TMD factorization is not expected to hold. In this work, we investigate the $\cos 2\phi_t$ asymmetry in a slightly different process, namely, when a J/ψ and a jet are observed almost back to back in ep collision. Only the WW-type gluon TMDs contribute in this process [42]. Here, the J/ψ produced can have large transverse momentum, as the soft scale required for the TMD factorization is provided by the total transverse momentum of the J/ψ-jet pair, which is smaller than their invariant mass as they are almost back to back [43]. In fact, by varying the invariant mass of the pair, one can also probe the TMDs over a wide range of scales and investigate the effect of TMD evolution on the asymmetry. In Ref. [42], the upper bound of the $\cos 2\phi_t$ asymmetry was investigated in this process, as well as the asymmetry in the small-x region. Here, we present a calculation of the asymmetry using some recent parametrization of the gluon TMDs and also investigate the effect of TMD evolution.

A widely used approach to calculate the amplitude of J/ψ production is based on an effective field theory called nonrelativistic QCD (NRQCD) [44–46]. Here, one assumes that the amplitude for the J/ψ production process can be factorized into a hard part where the $c\bar{c}$ pair is produced perturbatively and a soft part where the heavy quark pair hadronizes to form a J/ψ. The hadronization process is encoded in the long-distance matrix elements (LDMEs) [47], which are usually extracted using the data. The cross section is expressed as a double expansion in terms of the strong coupling α_s as well as the velocity parameter associated with the heavy quark v [48,49], in the limit $v \ll 1$. For charmonium, $v \approx 0.3$. The heavy quark pair in the hard process is produced in different states denoted by ${}^{2s+1}L_J^{(c)}$, where s denotes the spin of the pair (singlet or triplet), L is the orbital angular momentum, J is the total angular momentum, and (c) denotes the color configuration, which can be singlet or octet. The heavy quark pair produced in the hard process emits soft gluons to evolve into J/ψ. For the S-wave contribution, the dominant term in the limit $v \approx 0$ gives the result of the color singlet model [50,51], where the heavy quark pair in the hard process is assumed to be produced with the same quantum numbers as the J/ψ, and in the color singlet state. In our work, we include both color singlet (CS) and color octet (CO) contributions.

The paper is arranged as follows: In Sec. II, we present the TMD formalism adopted. In Sec. III, we investigate the effect of the TMD evolution on the asymmetries. In Secs. IV and V, we present two recent parametrizations of the gluon TMDs, based on the spectator model and a Gaussian parametrization, respectively. Numerical results are presented in Sec. VI. The conclusion is discussed in Sec. VII.

II. FORMALISM

We consider a semi-inclusive electroproduction of a J/ψ and a jet:

$$e^-(l) + p(\mathrm{P}) \to e^-(l') + J/\psi(\mathrm{P}_\psi) + \mathrm{jet}(\mathrm{P}_j) + X,$$

where the four-momenta of the particles are given in their corresponding round brackets. Here, both the incoming electron beam and the target proton are unpolarized with their respective momenta l and P. The kinematics of the process can be described in the following variables:

$$Q^2 = -q^2, \qquad s = (P+l)^2, \qquad W^2 = (P+q)^2, \tag{1}$$

$$x_B = \frac{Q^2}{2P\cdot q}, \qquad y = \frac{P\cdot q}{P\cdot l}, \qquad z = \frac{P\cdot \mathrm{P}_\psi}{P\cdot q}. \tag{2}$$

The virtuality of the scattering photon is given by Q^2, and s is the square of the electron-proton center of mass energy, whereas W is the invariant mass of photon-proton system. x_B is the Bjorken-x variable, y is the inelasticity variable that gives the fraction of the energy of the electron taken by the scattering virtual photon, and the variable z defines the fraction of energy of the photon carried by the outgoing J/ψ particle in the proton rest frame. We consider a virtual photon-proton center of mass frame where they move along $+z$ and $-z$ directions, respectively. To define the kinematics, we use the light-cone coordinate system. We use two lightlike vectors, one of which is chosen to be in the direction of the proton momentum, $P = n_-$ and the other $n = n_+$, such that $P\cdot n = 1$ and $n_-^2 = n_+^2 = 0$. In terms of these vectors, the momenta of the particles involved in the process can be written as follows.

Momenta of the initial proton and virtual photon can be expressed as

$$P^\mu = n_-^\mu + \frac{M_p^2}{2} n_+^\mu \approx n_-^\mu, \tag{3}$$

$$q^\mu = -x_B n_-^\mu + \frac{Q^2}{2x_B} n_+^\mu \approx -x_B P^\mu + (P\cdot q) n_+^\mu, \quad (4)$$

where M_p is the proton mass and $Q^2 = x_B y s$. The expressions for the incoming and outgoing lepton momenta can be written in terms of light-cone coordinates using the inelasticity variable y as

$$l^\mu = \frac{(1-y)x_B}{y} P^\mu + \frac{(P\cdot q)}{y} n^\mu + \frac{\sqrt{1-y}}{y} Q\hat{l}_\perp^\mu, \quad (5)$$

$$l'^\mu = l^\mu - q^\mu. \quad (6)$$

At the partonic level process, J/ψ can be produced either through the gluonic channel: $g+\gamma^\star \to J/\psi + g$, or through the quark (antiquark) channel: $q(\bar{q}) + \gamma^\star \to J/\psi + q(\bar{q})$. However, in the small-$x$ region, the gluonic channel dominates over the quark (antiquark) channel [42]. Hence, we have considered the contribution from the gluonic channel only in the following estimate of the asymmetry. The above processes contribute at the next-to-leading order in α_s and in the kinematic region $z < 1$. The outgoing energetic gluons produced in this process give the jet. Now, we can express the momentum of the initial gluon, p_g, the final J/ψ, and jet with momentum P_ψ and P_j, respectively, in terms of the lightlike vectors as

$$p_g^\mu = xP^\mu + (p_g\cdot P - M_p^2 x) n^\mu + \mathbf{p}_T^\mu \approx xP^\mu + \mathbf{p}_T^\mu, \quad (7)$$

$$\mathrm{P}_\psi^\mu = \frac{\mathbf{P}_{\psi\perp}^2 + M_\psi^2}{2zP\cdot q} P^\mu + z(P\cdot q) n^\mu + \mathbf{P}_{\psi\perp}^\mu, \quad (8)$$

$$\mathrm{P}_j^\mu = \frac{\mathbf{P}_{j\perp}^2}{2(1-z)P\cdot q} P^\mu + (1-z)(P\cdot q) n^\mu + \mathbf{P}_{j\perp}^\mu, \quad (9)$$

where x is the collinear momentum fraction of the initial gluon and $\mathbf{P}_{\psi\perp}$ and $\mathbf{P}_{j\perp}$ are the transverse momenta of J/ψ and jet, respectively. The incoming and the outgoing scattered lepton form the leptonic plane. All the azimuthal angles of the final state particles are defined with respect to the leptonic plane with $\phi_l = \phi_{l'} = 0$.

For the process under consideration, TMD factorization has not formally been proven yet, although it is expected to be valid. In our study, we have assumed TMD factorization. The total differential scattering cross section for the unpolarized process, $ep \to J/\psi$ jet X, can be written as [26]

$$d\sigma = \frac{1}{2s}\frac{d^3l'}{(2\pi)^3 2E_{l'}}\frac{d^3\mathrm{P}_\psi}{2E_\psi(2\pi)^3}\frac{d^3\mathrm{P}_j}{2E_j(2\pi)^3} \times \int dx d^2\mathbf{p}_T (2\pi)^4 \delta^4(q + p_g - \mathrm{P}_j - \mathrm{P}_\psi) \times \frac{1}{Q^4} L^{\mu\mu'}(l,q)\Phi_g^{\nu\nu'}(x,\mathbf{p}_T^2)\mathcal{M}_{\mu\nu}^{g\gamma^*\to J/\psi g}\mathcal{M}_{\mu'\nu'}^{*g\gamma^*\to J/\psi g}. \quad (10)$$

The function $\mathcal{M}_{\mu\nu}$ represents the scattering amplitude of J/ψ production in the photon-gluon fusion process: $\gamma^*(q) + g(p_g) \to Q\bar{Q}(\mathrm{P}_\psi) + g(\mathrm{P}_j)$ partonic subprocess. The leptonic tensor $L^{\mu\mu'}$ describes the electron-photon scattering and can be written as

$$L^{\mu\mu'} = e^2(-g^{\mu\mu'}Q^2 + 2(l^\mu l'^{\mu'} + l^{\mu'} l'^\mu)), \quad (11)$$

where e represents the electronic charge. The gluon correlator $\Phi_g^{\mu\nu'}(x,\mathbf{p}_T^2)$ describes the gluon content of the proton. At the leading twist, for the case of an unpolarized proton, it can be parametrized in terms of two TMD gluon distribution functions as [18]

$$\Phi_g^{\nu\nu'}(x,\mathbf{p}_T^2) = -\frac{1}{2x}\left\{ g_\perp^{\nu\nu'} f_1^g(x,\mathbf{p}_T^2) - \left(\frac{p_T^\nu p_T^{\nu'}}{M_p^2} + g_\perp^{\nu\nu'}\frac{\mathbf{p}_T^2}{2M_p^2}\right) h_1^{\perp g}(x,\mathbf{p}_T^2)\right\}. \quad (12)$$

Here, $g_\perp^{\nu\nu'} = g^{\nu\nu'} - P^\nu n^{\nu'}/P\cdot n - P^{\nu'} n^\nu / P\cdot n$. The quantities $f_1^g(x,\mathbf{p}_T^2)$ and $h_1^{\perp g}(x,\mathbf{p}_T^2)$ represent the unpolarized and linearly polarized gluon TMD, respectively.

A. J/ψ production in NRQCD framework

The Feynman diagrams for the dominant subprocess of photon-gluon fusion, which results in the production of a J/ψ and a jet, are shown in Fig. 1. The amplitude for the production of J/ψ within the NRQCD framework can be written as follows [36,51]:

$$\mathcal{M}(\gamma^* g \to Q\bar{Q}[^{2S+1}L_J^{(1,8)}]g) = \sum_{L_z S_z}\int \frac{d^3\mathbf{k}}{(2\pi)^3}\Psi_{LL_z}(\mathbf{k})\langle LL_z; SS_z|JJ_z\rangle \times \mathrm{Tr}[O(q,p_g,\mathrm{P}_\psi,k)\mathcal{P}_{SS_z}(\mathrm{P}_\psi,k)], \quad (13)$$

where k is the relative momentum of the heavy quark or the antiquark in the rest frame of the nonrelativistic quarkonium bound state, which is assumed to be very small as compared with the rest mass of the quarkonium. Here, $\Psi_{LL_z}(\mathbf{k})$ is the nonrelativistic bound-state wave function with orbital angular momentum L, L_z. The Clebsch-Gordan coefficients $\langle LL_z; SS_z|JJ_z\rangle$ project out their angular momentum. The mass of the quarkonium, M_ψ, is taken to be twice the heavy quark mass. The $O(q,p_g,\mathrm{P}_\psi,k)$ represents the amplitude for the production of the heavy quark antiquark pair $Q\bar{Q}$, without the inclusion of the polarization of the quark and antiquark. This can be calculated by considering the contributions from all the above Feynman diagrams and can be written as

$$O(q, p_g, \mathrm{P}_\psi, k) = \sum_{i=1}^{8} C_i O_i(q, p_g, \mathrm{P}_\psi, k), \tag{14}$$

where i denotes the contribution from the individual Feynman diagrams given in Fig. 1 and C_i corresponds to the color factor for each diagram. The $O_i(q, p_g, \mathrm{P}_\psi, k)$ for the above Feynman diagrams are written as

$$\begin{aligned}
O_1 &= 4g_s^2(ee_c)\varepsilon_g^{*\lambda}(\mathrm{P}_j)\gamma_\nu \frac{\not{\mathrm{P}}_\psi + 2\not{k} - 2\not{q} + M_\psi}{(\mathrm{P}_\psi + 2k - 2q)^2 - M_\psi^2} \\
&\times \gamma_\mu \frac{-\not{\mathrm{P}}_\psi + 2\not{k} - 2\not{\mathrm{P}}_j + M_\psi}{(\mathrm{P}_\psi - 2k + 2\mathrm{P}_j)^2 - M_\psi^2}\gamma_\lambda, \\
O_2 &= 4g_s^2(ee_c)\varepsilon_g^{*\lambda}(\mathrm{P}_j)\gamma_\lambda \frac{\not{\mathrm{P}}_\psi + 2\not{k} + 2\not{\mathrm{P}}_j + M_\psi}{(\mathrm{P}_\psi + 2k + 2\mathrm{P}_j)^2 - M_\psi^2} \\
&\times \gamma_\nu \frac{-\not{\mathrm{P}}_\psi + 2\not{k} + 2\not{p}_g + M_\psi}{(\mathrm{P}_\psi - 2k - 2p_g)^2 - M_\psi^2}\gamma_\mu, \\
O_3 &= 4g_s^2(ee_c)\varepsilon_g^{*\lambda}(\mathrm{P}_j)\gamma_\nu \frac{\not{\mathrm{P}}_\psi + 2\not{k} - 2\not{q} + M_\psi}{(\mathrm{P}_\psi + 2k - 2q)^2 - M_\psi^2} \\
&\times \gamma_\lambda \frac{-\not{\mathrm{P}}_\psi + 2\not{k} + 2\not{p}_g + M_\psi}{(\mathrm{P}_\psi - 2k - 2p_g)^2 - M_\psi^2}\gamma_\mu, \\
O_4 &= 4g_s^2(ee_c)\varepsilon_g^{*\lambda}(\mathrm{P}_j)\gamma_\nu \frac{\not{\mathrm{P}}_\psi + 2\not{k} - 2\not{q} + M_\psi}{(\mathrm{P}_\psi + 2k - 2q)^2 - M_\psi^2}\gamma^\chi \\
&\times \frac{[g_{\mu\lambda}(p_g + \mathrm{P}_j)_\chi + g_{\lambda\chi}(p_g - 2\mathrm{P}_j)_\mu + g_{\chi\mu}(\mathrm{P}_j - 2p_g)_\lambda]}{(p_g - \mathrm{P}_j)^2}.
\end{aligned} \tag{15}$$

The expressions for the remaining O_5, O_6, O_7, and O_8 can be obtained by reversing the fermionic current and replacing k to $-k$.

In the NRQCD framework, the outgoing $Q\bar{Q}$ pair can be formed in the color singlet (CS) state or in the color octet (CO) state. The color factor C_i corresponding to the CO case are given as [52]

$$\begin{aligned}
C_1 = C_6 = C_7 &= \sum_{jk} \langle 3j; \bar{3}k | 8c \rangle (t_a t_b)_{jk}, \\
C_2 = C_3 = C_5 &= \sum_{jk} \langle 3j; \bar{3}k | 8c \rangle (t_b t_a)_{jk}, \\
C_4 = C_8 &= \sum_{jk} \langle 3j; \bar{3}k | 8c \rangle i f_{abd} (t_d)_{jk}.
\end{aligned} \tag{16}$$

The SU(3) Clebsch-Gordan coefficients for CS and CO states are given by, respectively,

$$\langle 3j; \bar{3}k | 1 \rangle = \frac{\delta_{jk}}{\sqrt{N_c}}, \qquad \langle 3j; \bar{3}k | 8c \rangle = \sqrt{2}(t_c)_{jk}, \tag{17}$$

where N_c is the number of colors and t_c is the generator of SU(3) in the fundamental representation. Their properties are given by $\mathrm{Tr}[t_a t_b] = \delta_{ab}/2$ and $\mathrm{Tr}[t_a t_b t_c] = \frac{1}{4}(d_{abc} + i f_{abc})$. By using these relations along with the relation in Eq. (17), one obtains the color factors for individual Feynman diagrams for the $Q\bar{Q}$ formed in color octet states as

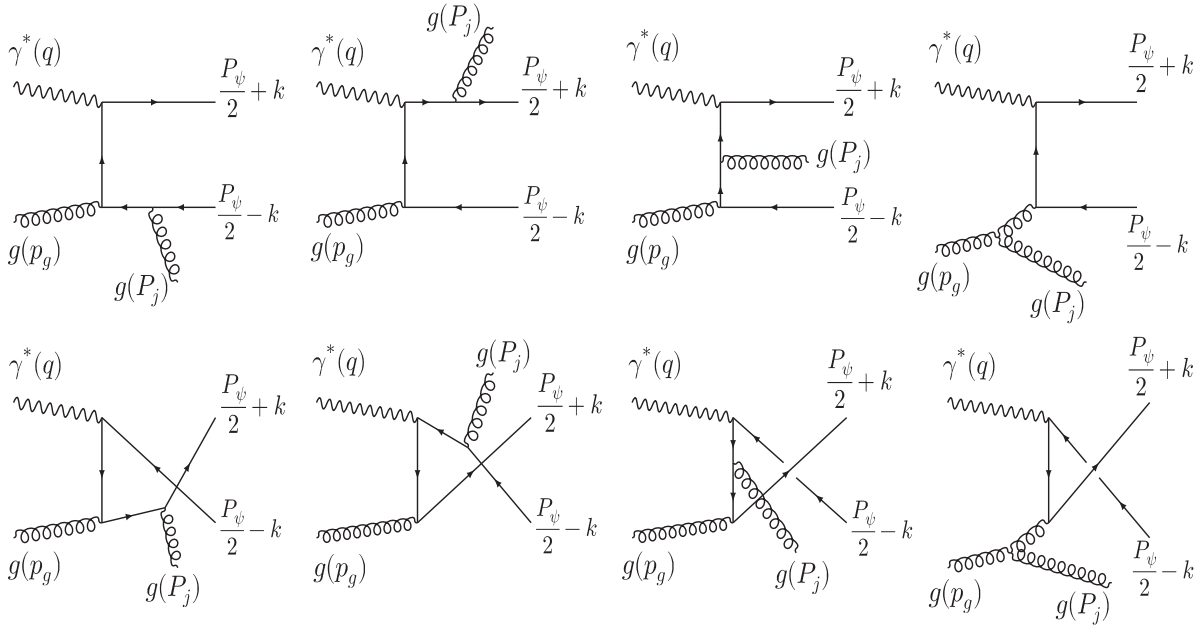

FIG. 1. Feynman diagrams for the partonic process $\gamma^*(q) + g(p_g) \to J/\psi(\mathrm{P}_\psi) + g(\mathrm{P}_j)$.

$$C_1 = C_6 = C_7 = \frac{\sqrt{2}}{4}(d_{abc} + if_{abc}),$$
$$C_2 = C_3 = C_5 = \frac{\sqrt{2}}{4}(d_{abc} - if_{abc}),$$
$$C_4 = C_8 = \frac{\sqrt{2}}{2} if_{abc}. \tag{18}$$

For the case of formation of a $Q\bar{Q}$ pair in the CS state, the color factors are given by

$$C_1 = C_2 = C_3 = C_5 = C_6 = C_7 = \frac{\delta_{ab}}{2\sqrt{N_c}}. \tag{19}$$

The spin projection operator for the bound state of the J/ψ includes the spinors of the heavy quark and antiquark, $c\bar{c}$, and is given as

$$\begin{aligned}\mathcal{P}_{SS_z}(\mathrm{P}_\psi, k) &= \sum_{s_1 s_2} \left\langle \frac{1}{2}s_1; \frac{1}{2}s_2 \middle| SS_z \right\rangle \\ &\times v\left(\frac{\mathrm{P}_\psi}{2} - k, s_1\right)\bar{u}\left(\frac{\mathrm{P}_\psi}{2} + k, s_2\right) \\ &= \frac{1}{4M_\psi^{3/2}}(-\not{\mathrm{P}}_\psi + 2\not{k} + M_\psi)\Pi_{SS_z}(\not{\mathrm{P}}_\psi + 2\not{k} + M_\psi) \\ &+ \mathcal{O}(k^2),\end{aligned} \tag{20}$$

where $\Pi_{SS_z} = \gamma^5$ for spin singlet ($S = 0$) and $\Pi_{SS_z} = \not{\varepsilon}_{S_z}(\mathrm{P}_\psi)$ for spin triplet ($S = 1$). The ε_{S_z} is the spin polarization vector of the outgoing $c\bar{c}$ pair.

Now, since, in the rest frame of the bound state, $k \ll \mathrm{P}_\psi$, one can Taylor expand the amplitude given in Eq. (13) around the $k = 0$ limit. In that expansion, the terms corresponding to k^0 give S-wave scattering amplitude ($L = 0,\ J = 0,\ 1$) and terms linear in k correspond to P-wave scattering ($L = 1,\ J = 0,\ 1,\ 2$), and the corresponding amplitudes are given as

$$\begin{aligned}&\mathcal{M}[^{2S+1}S_J^{(1,8)}](\mathrm{P}_\psi, k) \\ &= \frac{1}{\sqrt{4\pi}} R_0(0)\mathrm{Tr}[O(q, p_g, \mathrm{P}_\psi, k)\mathcal{P}_{SS_z}(\mathrm{P}_\psi, k)]\Big|_{k=0} \\ &= \frac{1}{\sqrt{4\pi}} R_0(0)\mathrm{Tr}[O(0)\mathcal{P}_{SS_z}(0)],\end{aligned} \tag{21}$$

$$\begin{aligned}&\mathcal{M}[^{2S+1}P_J^{(8)}](\mathrm{P}_\psi, k) \\ &= -i\sqrt{\frac{3}{4\pi}} R_1'(0)\sum_{L_z S_z} \varepsilon^\alpha_{L_z}(\mathrm{P}_\psi)\langle LL_z; SS_z|JJ_z\rangle \\ &\times \frac{\partial}{\partial k^\alpha}\mathrm{Tr}[O(q, p_g, \mathrm{P}_\psi, k)\mathcal{P}_{SS_z}(\mathrm{P}_\psi, k)]|_{k=0} \\ &= -i\sqrt{\frac{3}{4\pi}} R_1'(0)\sum_{L_z S_z} \varepsilon^\alpha_{L_z}(\mathrm{P}_\psi)\langle LL_z; SS_z|JJ_z\rangle \\ &\times \mathrm{Tr}[O_\alpha(0)\mathcal{P}_{SS_z}(0) + O(0)\mathcal{P}_{SS_z\alpha}(0)],\end{aligned} \tag{22}$$

where R_L represents the radial wave function and the shorthand notations used in the above expressions are

$$\begin{aligned}O(0) &= O(q, p_g, \mathrm{P}_\psi, k)|_{k=0}, \\ \mathcal{P}_{SS_z}(0) &= \mathcal{P}_{SS_z}(\mathrm{P}_\psi, k)|_{k=0},\end{aligned} \tag{23}$$

$$\begin{aligned}O_\alpha(0) &= \frac{\partial}{\partial k^\alpha} O(q, p_g, \mathrm{P}_\psi, k)\Big|_{k=0}, \\ \mathcal{P}_{SS_z\alpha}(0) &= \frac{\partial}{\partial k^\alpha}\mathcal{P}_{SS_z}(\mathrm{P}_\psi, k)\Big|_{k=0}.\end{aligned} \tag{24}$$

Following are the relations for the Clebsch-Gordan coefficient and the polarization vector of J/ψ, which we can use to calculate P-wave amplitudes [53]:

$$\sum_{L_z S_z}\langle LL_z; SS_z|JJ_z\rangle\varepsilon^\alpha_{S_z}(\mathrm{P}_\psi)\varepsilon^\beta_{L_z}(\mathrm{P}_\psi) = \sqrt{\frac{1}{3}}\left(g^{\alpha\beta} - \frac{\mathrm{P}_\psi^\alpha \mathrm{P}_\psi^\beta}{M_\psi^2}\right), \tag{25}$$

$$\begin{aligned}&\sum_{L_z S_z}\langle LL_z; SS_z|JJ_z\rangle\varepsilon^\alpha_{S_z}(\mathrm{P}_\psi)\varepsilon^\beta_{L_z}(\mathrm{P}_\psi) \\ &= -\frac{i}{M_\psi}\sqrt{\frac{1}{2}}\epsilon_{\delta\zeta\xi\varrho} g^{\xi\alpha} g^{\varrho\beta}\mathrm{P}_\psi^\delta \varepsilon^\zeta_{J_z}(\mathrm{P}_\psi),\end{aligned} \tag{26}$$

$$\sum_{L_z S_z}\langle LL_z; SS_z|JJ_z\rangle\varepsilon^\alpha_{S_z}(\mathrm{P}_\psi)\varepsilon^\beta_{L_z}(\mathrm{P}_\psi) = \varepsilon^{\alpha\beta}_{J_z}(\mathrm{P}_\psi). \tag{27}$$

The $\varepsilon^\alpha_{J_z}(\mathrm{P}_\psi)$ is the polarization vector corresponding to the $J = 1$ angular momentum state, that follows the current conservation and obeys the following relations [53]:

$$\varepsilon^\alpha_{J_z}(\mathrm{P}_\psi)\mathrm{P}_{\psi\alpha} = 0, \tag{28}$$

TABLE I. Numerical values for two different sets of LDMEs.

	$\langle 0\|\mathcal{O}_8^{J/\psi}(^1S_0)\|0\rangle$	$\langle 0\|\mathcal{O}_8^{J/\psi}(^3S_1)\|0\rangle$	$\langle 0\|\mathcal{O}_1^{J/\psi}(^3S_1)\|0\rangle$	$\langle 0\|\mathcal{O}_8^{J/\psi}(^3P_0)\|0\rangle/m_c^2$	
Ref. [54]	1.8 ± 0.87	0.13 ± 0.13	1.2×10^2	1.8 ± 0.87	$\times 10^{-2}$ GeV^3
Ref. [55]	8.9 ± 0.98	0.30 ± 0.12	1.2×10^2	0.56 ± 0.21	$\times 10^{-2}$ GeV^3

$$\sum_{J_z} \varepsilon^{\alpha}_{J_z}(\mathrm{P}_\psi)\varepsilon^{*\beta}_{J_z}(\mathrm{P}_\psi) = \left(-g^{\alpha\beta} + \frac{\mathrm{P}^{\alpha}_{\psi}\mathrm{P}^{\beta}_{\psi}}{M^2_\psi}\right) = \mathcal{Q}^{\alpha\beta}. \quad (29)$$

The $\varepsilon^{\alpha\beta}_{J_z}(\mathrm{P}_\psi)$ is the polarization tensor corresponding to $J = 2$ which is symmetric in the Lorentz indices and follows the relations [53]

$$\varepsilon^{\alpha\beta}_{J_z}(\mathrm{P}_\psi) = \varepsilon^{\beta\alpha}_{J_z}(\mathrm{P}_\psi),\ \ \varepsilon^{\alpha}_{J_z\alpha}(\mathrm{P}_\psi) = 0,\ \ \varepsilon^{\alpha}_{J_z}(\mathrm{P}_\psi)\mathrm{P}_{\psi\alpha} = 0,$$
$$\varepsilon^{\alpha\beta}_{J_z}(\mathrm{P}_\psi)\varepsilon^{*\mu\nu}_{J_z}(\mathrm{P}_\psi) = \frac{1}{2}[\mathcal{Q}^{\alpha\mu}\mathcal{Q}^{\beta\nu} + \mathcal{Q}^{\alpha\nu}\mathcal{Q}^{\beta\mu}] - \frac{1}{3}[\mathcal{Q}^{\alpha\beta}\mathcal{Q}^{\mu\nu}]. \quad (30)$$

The radial wave function and its derivative evaluated at origin $R_0(0)$, $R'_1(0)$ given in Eqs. (21) and (22) are related to LDMEs by the following equations [42]:

$$\langle 0|\mathcal{O}^{J/\psi}_1(^{2S+1}S_J)|0\rangle = \frac{N_c}{2\pi}(2J+1)|R_0(0)|^2, \quad (31)$$

$$\langle 0|\mathcal{O}^{J/\psi}_8(^{2S+1}S_J)|0\rangle = \frac{2}{\pi}(2J+1)|R_0(0)|^2, \quad (32)$$

$$\langle 0|\mathcal{O}^{J/\psi}_8(^{3}P_J)|0\rangle = \frac{2N_c}{\pi}(2J+1)|R'_1(0)|^2. \quad (33)$$

The two different sets of LDMEs that we have used in our numerical calculation are given in Table I. Now, using the aforementioned formalism, together with the symmetry relations among the amplitudes corresponding to different Feynman diagrams for each state, which have been calculated in Ref. [52], we could write the amplitude for the CS state ($^3S^{(1)}_1$) and CO states ($^3S^{(8)}_1$, $^1S^{(8)}_0$, $^3P^{(8)}_{J(0,1,2)}$) as follows.

B. $^3S^{(1,8)}_1$ amplitude

The final expression for the $^3S^{(1)}_1$ state and $^3S^{(8)}_1$ state can be written as

$$\mathcal{M}[^3S^{(1)}_1](\mathrm{P}_\psi, p_g) = \frac{1}{4\sqrt{\pi M_\psi}}R_0(0) \times \frac{\delta_{ab}}{2\sqrt{N_c}}\mathrm{Tr}\left[\sum_{i=1}^{3} O_i(0)(\not{\mathrm{P}}_\psi + M_\psi)\not{\epsilon}_{S_z}\right], \quad (34)$$

$$\mathcal{M}[^3S^{(8)}_1](\mathrm{P}_\psi, p_g) = \frac{1}{4\sqrt{\pi M_\psi}}R_0(0) \times \frac{\sqrt{2}}{2}d_{abc}\mathrm{Tr}\left[\sum_{i=1}^{3} O_i(0)(\not{\mathrm{P}}_\psi + M_\psi)\not{\epsilon}_{S_z}\right], \quad (35)$$

where $\sum_{i=1}^{3} O_i(0)$ is given as

$$\sum_{i=1}^{3} O_i(0) = 4g_s^2(ee_c)\varepsilon^{*\lambda}_g\left[\frac{\gamma_\nu(\not{\mathrm{P}}_\psi - 2\not{q} + M_\psi)\gamma_\mu(-\not{\mathrm{P}}_\psi - 2\not{\mathrm{P}}_j + M_\psi)\gamma_\lambda}{(s - M^2_\psi)(u - M^2_\psi + q^2)} + \frac{\gamma_\lambda(\not{\mathrm{P}}_\psi + 2\not{\mathrm{P}}_j + M_\psi)\gamma_\nu(-\not{\mathrm{P}}_\psi + 2\not{p}_g + M_\psi)\gamma_\mu}{(s - M^2_\psi)(t - M^2_\psi)} + \frac{\gamma_\nu(\not{\mathrm{P}}_\psi - 2\not{q} + M_\psi)\gamma_\lambda(-\not{\mathrm{P}}_\psi + 2\not{p}_g + M_\psi)\gamma_\mu}{(t - M^2_\psi)(u - M^2_\psi + q^2)}\right]. \quad (36)$$

The symmetry relations, given in Ref. [52], lead to the cancellation of contributions from Feynman diagrams 4 and 8 for the $^3S^{(1,8)}_1$ amplitude.

C. $^1S^{(8)}_0$ amplitude

The total amplitude for the $^1S^{(8)}_0$ state can be written as

$$\mathcal{M}[^1S^{(8)}_0](\mathrm{P}_\psi, p_g) = \frac{1}{4\sqrt{\pi M_\psi}}R_0(0)i\frac{\sqrt{2}}{2}f_{abc}\mathrm{Tr}[(O_1(0) - O_2(0) - O_3(0) + 2O_4(0))(\not{\mathrm{P}}_\psi + M_\psi)\gamma_5]. \quad (37)$$

$O_1(0)$, $O_2(0)$, and $O_3(0)$ are given in Eq. (36), and

$$O_4(0) = g_s^2(ee_c)\varepsilon^{*\lambda}_g\frac{\gamma_\nu(\not{\mathrm{P}}_\psi - 2\not{q} + M_\psi)\gamma^\chi}{u(u - M^2_\psi)}[g_{\mu\lambda}(p_g + \mathrm{P}_j)_\chi + g_{\lambda\chi}(p_g - 2\mathrm{P}_j)_\mu + g_{\chi\mu}(\mathrm{P}_j - 2p_g)_\lambda]. \quad (38)$$

D. $^3P_J^{(8)}$ amplitude

The $^3P_J^{(8)}$ amplitude can be written as [52]

$$\mathcal{M}[^3\mathcal{P}_J^{(8)}](\mathrm{P}_\psi, p_g) = \frac{\sqrt{2}}{2} f_{abc}\sqrt{\frac{3}{4\pi}}R_1'(0) \times \sum_{L_z S_z} \varepsilon^{\alpha}_{L_z}(\mathrm{P}_\psi)\langle LL_z; SS_z|JJ_z\rangle \times \mathrm{Tr}[(O_{1\alpha}(0) - O_{2\alpha}(0) - O_{3\alpha}(0) + 2O_{4\alpha}(0))\mathcal{P}_{SS_z}(0) + (O_1(0) - O_2(0) - O_3(0) + 2O_4(0))\mathcal{P}_{SS_z\alpha}(0)]. \quad (39)$$

E. Total differential cross section and the asymmetry

The structure of the differential cross section as defined in Eq. (10) has a contraction of tensors which can be schematically written as

$$\mathfrak{M}_i\mathfrak{M}_j = L^{\mu\mu'}(l,q)\Phi_g^{\nu\nu'}(x,\mathbf{p}_T)\mathcal{M}_{i\mu\nu}\mathcal{M}_{j\mu'\nu'}, \quad (40)$$

where $i,\ j = 1,\ 2,\ 3,\ 4$ corresponds to the Feynman diagrams given in Fig. 1 and we have $\mathfrak{M}_i\mathfrak{M}_j = \mathfrak{M}_j\mathfrak{M}_i$ for $i \neq j$. We have already defined all tensors in the above convolution, and contributions to the amplitudes come from all the CS and CO states $(^3S_1^{(1,8)}, {}^1S_0^{(8)}, {}^3P_{J(0,1,2)}^{(8)})$. We have summed over all the polarization states of the outgoing gluon using the relation given as

$$\sum_{\lambda_a=1}^{2}\varepsilon_\mu^{\lambda_a}\varepsilon_{\mu'}^{\lambda_a} = -g_{\mu\mu'} + \frac{\mathrm{P}_{j\mu}n_{\psi\mu'} + \mathrm{P}_{j\mu'}n_{\psi\mu}}{\mathrm{P}_j\cdot n_\psi} - \frac{\mathrm{P}_{j\mu}\mathrm{P}_{j\mu'}}{(\mathrm{P}_j\cdot n_\psi)^2}, \quad (41)$$

where $n_{\psi\mu} = \mathrm{P}_{\psi\mu}/M_\psi$. We use the frame where the incoming virtual photon and proton move along the z axis. The azimuthal angles of the lepton scattering plane are defined as $\phi_l = \phi_{l'} = 0$. We integrate out the azimuthal angle of the final lepton ℓ' [56], and we can write

$$\frac{\mathrm{d}^3\ell'}{(2\pi)^3 2E_{\ell'}} = \frac{\mathrm{d}Q^2\mathrm{d}y}{16\pi^2}. \quad (42)$$

Moreover, for the other phase factors, one can write

$$\frac{\mathrm{d}^3\mathrm{P}_\psi}{(2\pi)^3 2E_\psi} = \frac{\mathrm{d}z\mathrm{d}^2\mathbf{P}_{\psi\perp}}{(2\pi)^3 2z}, \qquad \frac{\mathrm{d}^3\mathrm{P}_j}{(2\pi)^3 2E_j} = \frac{\mathrm{d}\bar{z}\mathrm{d}^2\mathbf{P}_{j\perp}}{(2\pi)^3 2\bar{z}}, \quad (43)$$

and conservation of the four-momenta can be written as

$$\delta^4(q + p_g - \mathrm{P}_\psi - \mathrm{P}_j) = \frac{2}{ys}\delta(1-z-\bar{z})\delta\left(x - \frac{\bar{z}(M^2 + \mathbf{P}_{\psi\perp}^2) + z\mathbf{P}_{j\perp}^2 + z\bar{z}Q^2}{z(1-z)ys}\right) \times \delta^2(\mathbf{p}_T - \mathbf{P}_{j\perp} - \mathbf{P}_{\psi\perp}), \quad (44)$$

where we have used the relation $Q^2 = x_B ys$. Now, we define the sum and difference of the transverse momentum of J/ψ and jet as

$$\mathbf{q}_t \equiv \mathbf{P}_{\psi\perp} + \mathbf{P}_{j\perp}, \qquad \mathbf{K}_t \equiv \frac{\mathbf{P}_{\psi\perp} - \mathbf{P}_{j\perp}}{2}. \quad (45)$$

From Eq. (44), we have $\bar{z} = (1-z)$ and $\mathbf{q}_t = \mathbf{p}_T$. We use TMD factorization in the kinematic region $|\mathbf{q}_t| \ll |\mathbf{K}_t|$. This leads to the situation where the outgoing J/ψ and jet are almost back to back in the transverse plane, i.e., the xy plane, with respect to the virtual photon-proton colliding axis, i.e., the z axis, thus allowing us to set $\mathbf{K}_t \simeq \mathbf{P}_{\psi\perp} \simeq -\mathbf{P}_{j\perp}$. ϕ_t and $\phi_\perp$ are the azimuthal angles, respectively, for $\mathbf{q}_t$ and $\mathbf{K}_t$ and are defined with respect to the leptonic plane as illustrated in Fig. 2. Finally, integrating over $\bar{z}$, $\mathbf{p}_T$, and x, the differential cross section, in Eq. (10), as a function of z, y, x_B, $\mathbf{q}_t$, and $\mathbf{K}_t$ can be rewritten as

$$\frac{\mathrm{d}\sigma}{\mathrm{d}z\mathrm{d}y\mathrm{d}x_B\mathrm{d}^2\mathbf{q}_t\mathrm{d}^2\mathbf{K}_t} = \frac{1}{(2\pi)^4}\frac{1}{16sz(1-z)Q^4}\sum_{i,j}\mathfrak{M}_i\mathfrak{M}_j. \quad (46)$$

In the following calculation, we have kept only the zeroth- and first-order terms in $(\frac{\mathbf{q}_t^2}{M_P^2})$. Thus, we obtain the total differential cross section [42]

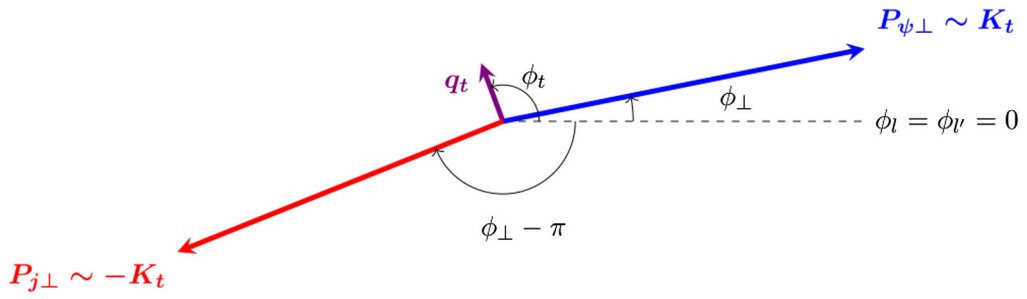

FIG. 2. The schematic representation of back-to-back J/ψ and jet production in the transverse plane.

$$\frac{d\sigma}{dz dy dx_B d^2\mathbf{q}_t d^2\mathbf{K}_t} = \frac{1}{(2\pi)^4}\frac{1}{16sz(1-z)Q^4}\Big\{(\mathbb{A}_0 + \mathbb{A}_1\cos\phi_\perp + \mathbb{A}_2\cos 2\phi_\perp) f_1^g(x,\mathbf{q}_t^2) + \frac{\mathbf{q}_t^2}{M_P^2} h_1^{\perp g}(x,\mathbf{q}_t^2)(\mathbb{B}_0\cos 2\phi_t + \mathbb{B}_1\cos(2\phi_t-\phi_\perp) + \mathbb{B}_2\cos 2(\phi_t-\phi_\perp) + \mathbb{B}_3\cos(2\phi_t-3\phi_\perp) + \mathbb{B}_4\cos(2\phi_t-4\phi_\perp))\Big\}. \quad (47)$$

The analytic expressions of the coefficients $\mathbb{A}_i$'s and $\mathbb{B}_i$'s are very lengthy, which we have not included in this article. They are available upon request.

The TMDs come with various azimuthal modulations. These modulations can be used to extract information about the ratio of TMDs. This can be done by defining the asymmetries as [42]

$$A^{\mathcal{W}(\phi_S,\phi_t)} \equiv 2\frac{\int d\phi_S d\phi_t d\phi_\perp \mathcal{W}(\phi_S,\phi_t) d\sigma(\phi_S,\phi_t,\phi_\perp)}{\int d\phi_S d\phi_t d\phi_\perp d\sigma(\phi_S,\phi_t,\phi_\perp)}. \quad (48)$$

Here, we are interested in one particular asymmetry, i.e., $\cos 2\phi_t$ asymmetry, to extract the linearly polarized gluon TMD. This can be written as

$$\langle\cos 2\phi_t\rangle \equiv A^{\cos 2\phi_t} = 2\frac{\int d\phi_t d\phi_\perp \cos 2\phi_t d\sigma(\phi_t,\phi_\perp)}{\int d\phi_t d\phi_\perp d\sigma(\phi_t,\phi_\perp)}. \quad (49)$$

Now, by plugging the differential scattering cross section from Eq. (47) into the above equation, we get the $\cos 2\phi_t$ asymmetry as a function of z, y, x_B, and K_t:

$$\langle\cos 2\phi_t\rangle \equiv A^{\cos 2\phi_t} = \frac{\int q_t dq_t \frac{\mathbf{q}_t^2}{M_p^2}\mathbb{B}_0 h_1^{\perp g}(x,\mathbf{q}_t^2)}{\int q_t dq_t \mathbb{A}_0 f_1^g(x,\mathbf{q}_t^2)}. \quad (50)$$

For estimating the $\cos 2\phi_t$ asymmetry numerically, we have used two recent parametrizations of the gluon TMDs and also estimated the effect of TMD evolution. The following section gives the details of the TMD evolution formalism used.

III. TMD EVOLUTION

The evolution of the TMDs [57,58] with the scale affects the asymmetries measured in the energies of different experiments, and it is important to estimate the effect of this evolution to obtain the angular asymmetries of produced hadrons measured by the HERMES, COMPASS, and JLab as well as the future EIC experiments at different energies. The TMD evolution is usually studied in the impact parameter space [57]. The impact-parameter-dependent TMDs can be written as Fourier transforms of the TMDs:

$$\hat{f}(x,\mathbf{b}_t^2;Q_f^2) = \frac{1}{2\pi}\int d^2\mathbf{q}_t e^{i\mathbf{q}_t\cdot\mathbf{b}_t} f(x,\mathbf{q}_t^2,Q_f^2). \quad (51)$$

In the TMD evolution approach, TMDs not only evolve with the intrinsic transverse momentum of the parton but also evolve with the probing scale. The expression for TMD evolution at a given final scale Q_f can be obtained by solving the Collins-Soper evolution equation and renormalization group equation. Using this approach, the expression for the gluon TMD in the impact parameter space can be written as [7,59,60]

$$\hat{f}(x,\mathbf{b}_t^2,Q_f^2) = \frac{1}{2\pi}\sum_{p=q,\bar{q},g}(C_{g/p}\otimes f_1^p)(x,Q_i^2) \times e^{-\frac{1}{2}S_A(\mathbf{b}_t^2,Q_f^2,Q_i^2)} e^{-S_{np}(\mathbf{b}_t^2,Q_f^2)}, \quad (52)$$

where Q_i is the initial scale of TMD, defined in terms of b_t as $Q_i = 2e^{-\gamma_E}/b_t$ and $\gamma_E \approx 0.577$. $C_{g/p}$ are coefficient functions, and $f_1^p(x,Q^2)$ are collinear parton distributions for a species of partons like quark and antiquark or gluon. The exponents S_A and S_{np} are the perturbative and nonperturbative Sudakov factors, respectively. We note that the Sudakov factor S_A is spin independent and, thus, the same for all (un) polarized TMDs [35,61]. As stated before, a formal proof of TMD factorization for this process remains to be done, and here we study the effect of TMD evolution on the asymmetry assuming such factorization. The subsections below contain a description of the TMD evolution formalism used and the relevant formulas.

A. Coefficient functions and perturbative Sudakov factor

The coefficient function can be written as a series of strong coupling constant α_s [62]:

$$C_{g/p}(x,Q_i) = \delta_{gp}\delta(1-x) + \sum_{k=1}^{\infty}\sum_{p=g.q.\bar{q}} C_{g/p}^k(x)\left(\frac{\alpha_s(Q_i)}{\pi}\right)^k. \quad (53)$$

The Sudakov factor as the leading order of α_s can be written as [62]

$$S_A(\mathbf{b}_t^2, Q_f^2, Q_i^2) = \frac{C_A}{\pi}\int_{Q_i^2}^{Q_f^2}\frac{d\eta^2}{\eta^2}\alpha_s(\eta)\left(\log\frac{Q_f^2}{\eta^2} - \frac{11-2n_f/C_A}{6}\right) = \frac{C_A}{\pi}\alpha_s\left(\frac{1}{2}\log^2\frac{Q_f^2}{Q_i^2} - \frac{11-2n_f/C_A}{6}\log\frac{Q_f^2}{Q_i^2}\right). \tag{54}$$

The running of the coupling α_s is ignored in Eq. (54), because it starts at α_s^2. The $C_A = N_c$, n_f denotes the number of active flavors. In $\mathrm{b}_t \ll 1/\Lambda_{\mathrm{QCD}}$, the Sudakov factor can be Taylor expanded. Furthermore, by substituting the expressions from Eqs. (53) and (54), the unpolarized gluon TMD at LO without a nonperturbative Sudakov factor is given as [62]

$$\hat{f}_1^g(x, \mathbf{b}_t^2; Q_f^2) = \frac{1}{2\pi}\left\{f_1^g(x, Q_i^2) - \frac{\alpha_s}{2\pi}\left(\left[\frac{C_A}{2}\log^2\frac{Q_f^2}{Q_i^2} - \frac{11-2n_f/C_A}{6}\log\frac{Q_f^2}{Q_i^2}\right]f_1^g(x, Q_i^2) - 2\sum_p (C_{g/p}^1 \otimes f_1^p)(x, Q_i^2)\right)\right\}. \tag{55}$$

Scale evolution of the collinear parton distribution functions (PDFs) are given by the Dokshitzer-Gribov-Lipatov-Altarelli-Parisi (DGLAP) equation. Using this evolution equation, one can evolve $f_1^g(x, Q_i^2)$ from the initial scale Q_i to the final scale Q_f where $Q_i < Q_f$:

$$f_1^g(x, Q_i^2) = f_1^g(x, Q_f^2) - \frac{\alpha_s}{2\pi}(P_{gg} \otimes f_1^g + P_{gi} \otimes f_1^i)(x, Q_f^2) \times \log\frac{Q_f^2}{Q_i^2} + \mathcal{O}(\alpha_s^2). \tag{56}$$

Here, P_{gg} and P_{gi} are leading-order splitting functions, which are given as

$$P_{gg}(\hat{x}) = 2C_A\left[\frac{\hat{x}}{(1-\hat{x})_+} + \frac{1-\hat{x}}{\hat{x}} + \hat{x}(1-\hat{x})\right] + \delta(1-\hat{x})\frac{11C_A - 4n_f T_R}{6}, \tag{57}$$

$$P_{gq}(\hat{x}) = P_{g\bar{q}}(\hat{x}) = C_F\frac{1+(1-\hat{x})^2}{\hat{x}}, \tag{58}$$

where $C_F = (N_c^2 - 1)/2N_c$ and $T_R = 1/2$. In Eq. (57), the first term involves the plus prescription and, thus, avoids an infrared divergence because of $(1-\hat{x})$ in the denominator. The plus prescription is given as [62]

$$\int_y^1 dz\frac{G(z)}{(1-z)_+} = \int_y^1 dz\frac{G(z)-G(1)}{1-z} - G(1)\log\left(\frac{1}{1-z}\right). \tag{59}$$

The $\otimes$ symbol denotes convolution of the two quantities;

$$(P \otimes f_1^g)(x, Q^2) = \int_x^1 \frac{d\hat{x}}{\hat{x}}P(\hat{x}, Q^2)f\left(\frac{x}{\hat{x}}, Q^2\right). \tag{60}$$

After convolution and substitution of Eq. (56) in Eq. (55), we have the final equation for the unpolarized gluon TMD as

$$\hat{f}_1^g(x, \mathbf{b}_t^2; Q_f^2) = \frac{1}{2\pi}\left\{f_1^g(x, Q_f^2) - \frac{\alpha_s}{2\pi}\left[\left(\frac{C_A}{2}\log^2\frac{Q_f^2}{Q_i^2} - \frac{11C_A - 2n_f}{6}\log\frac{Q_f^2}{Q_i^2}\right)f_1^g(x, Q_f^2) + (P_{gg} \otimes f_1^g + P_{gi} \otimes f_1^i)(x, Q_f^2)\log\frac{Q_f^2}{Q_i^2} - 2f_1^g(x, Q_f^2)\right]\right\}. \tag{61}$$

Now, we can write the above equation in the $\mathbf{q}_t$ space by making one-to-one correspondence between the functions in impact parameter and momentum space using a general formula [35,63,64]:

$$\hat{f}^{(n)}(x, \mathbf{b}_t^2) \equiv \frac{2\pi n!}{M^{2n}}\int_0^\infty d\mathrm{q_t}\mathrm{q_t}\left(\frac{\mathrm{q_t}}{\mathrm{b_t}}\right)^n J_n(\mathrm{q_t}\mathrm{b_t})f(x, \mathbf{q}_t^2), \tag{62}$$

where n is the rank of function in $\mathbf{q_t}$ space. Since the unpolarized vector-meson production generally has a rank-zero structure, we can write the unpolarized gluon TMD together with the nonperturbative Sudakov factor in terms of $\mathbf{q_t}$ space as

$$f_1^g(x, \mathbf{q}_t^2) = \frac{1}{2\pi}\int_0^\infty \mathrm{b}_t d\mathrm{b}_t J_0(\mathrm{b}_t\mathrm{q}_t)\left\{f_1^g(x, Q_f^2) - \frac{\alpha_s}{2\pi}\left[\left(\frac{C_A}{2}\log^2\frac{Q_f^2}{Q_i^2} - \frac{11C_A - 2n_f}{6}\log\frac{Q_f^2}{Q_i^2}\right)f_1^g(x, Q_f^2) + (P_{gg} \otimes f_1^g + P_{gi} \otimes f_1^i)(x, Q_f^2)\log\frac{Q_f^2}{Q_i^2} - 2f_1^g(x, Q_f^2)\right]\right\} \times e^{-S_{np}(\mathbf{b}_t^2)}. \tag{63}$$

Now let us write the expression for the linearly polarized gluon distribution function $h_1^{\perp g}(x, \mathbf{b}_t^2)$. The perturbative tail of $h_1^{\perp g}$ can be computed in the same way as the perturbative tail of f_1^g, with the key difference that its expansion in powers of the QCD coupling constant begins at $O(\alpha_s)$. Using Eq. (3.13) in Ref. [62] and then performing the Fourier transformation using Eq. (62), we write the linearly polarized gluon distribution at LO in terms of the unpolarized collinear PDFs $f_1^q(\hat{x}, Q_f^2)$ in the $\mathbf{b}_t$ space as

$$h_1^{\perp g(2)}(x, \mathbf{b}_t^2; Q_f^2) = \frac{2\alpha_S}{\pi^2 M_p^2}\frac{1}{\mathbf{b}_t^2}\left[C_A \int_x^1 \frac{d\hat{x}}{\hat{x}}\left(\frac{\hat{x}}{x}-1\right) f_1^g(\hat{x}, Q_f^2) + C_F \sum_{p=q,\bar{q}} \int_x^1 \frac{d\hat{x}}{\hat{x}}\left(\frac{\hat{x}}{x}-1\right) f_1^p(\hat{x}, Q_f^2)\right]. \tag{64}$$

Here, we have used the general formula for the Bessel integral [65]:

$$\int_0^\infty dk k^{\lambda-1} J_\nu(kx) = 2^{\lambda-1} x^{-\lambda} \frac{\Gamma(1/2(\nu+\lambda))}{\Gamma(1/2(2+\nu+\lambda))}, \tag{65}$$

where $J_\nu(z)$ is the Bessel function of the first kind of the order of ν. The q_t dependence for $h_1^{\perp g}$ in the gluon correlator has a rank-two tensor structure in the noncontracted transverse momentum; thus, we could write the linearly polarized gluon TMD $h_1^{\perp g}$ in the $\mathbf{q}_t$ space as

$$\frac{\mathbf{q}_t^2}{M_p^2} h_1^{\perp g(2)}(x, \mathbf{q}_t^2) = \frac{\alpha_s}{\pi^2}\int_0^\infty d\mathrm{b_t} \mathrm{b_t} J_2(\mathrm{q_t b_t})\left[C_A \int_x^1 \frac{d\hat{x}}{\hat{x}}\left(\frac{\hat{x}}{x}-1\right) f_1^g(\hat{x}, Q_f^2) + C_F \sum_{p=q,\bar{q}} \int_x^1 \frac{d\hat{x}}{\hat{x}}\left(\frac{\hat{x}}{x}-1\right) f_1^p(\hat{x}, Q_f^2)\right] \times e^{-S_{np}(\mathbf{b_t}^2)}. \tag{66}$$

B. Nonperturbative Sudakov factor

In the above Eqs. (63) and (66), the perturbative part is strictly valid in the perturbative domain, which means low b_t (or $\mathrm{b}_t \ll 1/\Lambda_{\mathrm{QCD}}$). However, in order to perform the corresponding Fourier transform, we need to integrate the expression from small to large b_t. As a result, the perturbative expression for the Sudakov factor given above should not be used alone; rather, one needs to introduce a nonperturbative Sudakov factor, and this should suppress the large b_t domain. The functional form of the nonperturbative Sudakov factor is constrained by two conditions, one of which is it has to be equal to 1 for $\mathrm{b}_t = 0$ and for large b_t it is supposed to decrease monotonically and ultimately should vanish. The functional form attributed to S_{np} is quadratic in b_t with $e^{-S_{np}}$ reaching 0 within a certain value of b_t called $\mathrm{b}_{t\,\mathrm{lim}}$. However, when b_t gets too small, the lower scale $Q_i = 2e^{-\gamma_E}/\mathrm{b}_t$ will be larger than final scale Q_f, and, hence, we expect the evolution should stop. This could be resolved by taking a b_t prescription as given below [66]:

$$b_{t\star}(\mathrm{b}_c(\mathrm{b}_t)) = \frac{\mathrm{b}_c(\mathrm{b}_t)}{\sqrt{1+\frac{\mathrm{b}_c(\mathrm{b}_t)}{b_{t\,\mathrm{max}}}}}, \tag{67}$$

where

$$\mathrm{b}_c = \sqrt{\mathrm{b}_t^2 + \left(\frac{2e^{-\gamma_E}}{Q_f}\right)^2}.$$

This prescription constrains the $Q_i(\mathrm{b}_t) = 2\gamma_E/b_{t\star}(\mathrm{b}_t)$ range in between $2\gamma_E/\mathrm{b}_{t\,\mathrm{max}}$ (for $\mathrm{b}_t \to \infty$) and Q_f (for $\mathrm{b}_t \to 0$). Motivated by Ref. [66], we choose the Gaussian behavior of $e^{-S_{np}}$ as

$$S_{np} = \frac{A}{2}\log\left(\frac{Q_f}{Q_{np}}\right)\mathrm{b}_c^2, \qquad Q_{np} = 1\ \mathrm{GeV}. \tag{68}$$

The parameter A controls the width of the nonperturbative Sudakov factor for a particular Q_f. In this calculation, we have taken the final scale as $Q_f = \sqrt{M_\psi^2 + \mathrm{K}_t^2}$. We have taken $A = 2.3\ \mathrm{GeV}^2$, which is calculated for $\mathrm{K}_t = 1$ GeV. The K_t dependence present in Q_f does not affect the value of A, as K_t increases the $e^{-S_{np}}$ remains below the convergence criteria at the given $\mathrm{b}_{t\,\mathrm{lim}}$. The value of $\mathrm{b}_{t\,\mathrm{max}}$ for the following numerical study is $1.5\ \mathrm{GeV}^{-1}$, which is consistent with Ref. [66], the Collins-Soper-Sterman formalism given for Z boson production [67], and the Collins-Soper-Sterman formalism implemented by Ref. [68]. Below, we present two recent parametrizations of the gluon TMDs that we have used.

IV. SPECTATOR MODEL

In this section, we discuss a recent parametrization of the gluon TMDs based on a spectator model [69]. According to this model, the remnant after the gluon emission from the nucleon is treated as a single spectator particle, which is on shell, with mass M_X. The mass can take a range of values given by a spectral function. The nucleon-gluon-spectator coupling is encoded in an effective vertex that contains two form factors. The expression for a given TMD reads as

$$F^g(x, \mathbf{q}_t^2) = \int_M^\infty dM_X \rho_X(M_X) \hat{F}^g(x, \mathbf{q}_t^2; M_X). \tag{69}$$

Here, $\rho_X(M_X)$ is the spectral function and can be written as

$$\rho_X(M_X) = \mu^{2a}\left[\frac{A}{B+\mu^{2b}} + \frac{C}{\pi\sigma} e^{-\frac{(M_X-D)^2}{\sigma^2}}\right], \tag{70}$$

where $\mu = M_X^2 - M^2$ and $\{X\} \equiv \{A, B, a, b, C, D, \sigma\}$ are free parameters. The parameter B in the above equation is set at $B = 2.1$, and M_X can take real values in the continuous range according to the above spectral function. The nucleon mass M is taken to be 1. The parameters a and b have a strong influence on the spectral function; at larger M_X, its asymptotic trend depends on the sign of the difference $a - b$ [69]. For $a - b < 0$, the value of ρ_X approaches zero for large M_X. We consider integration in Eq. (69) over the range $1 < M_X < 10$ GeV. The value of different parameters that we used for our numerical results are given in Table II below. These model parameters have been fixed by fitting the NNPDF data at scale $Q = 1.64$ GeV [69]. We assumed the same set of parameters to probe the TMDs at $Q = \sqrt{M_\psi^2 + \mathrm{K}_t^2}$. In this model, we do not have direct inference of scale dependency on the TMDs unlike the case of Gaussian parametrization. However, the longitudinal momentum fraction x depends on Q, but going from some low $Q = 1.64$ GeV to some relatively large $Q = \sqrt{M_\psi + \mathrm{K}_t^2}$ ($\approx$6.75 GeV for $M_\psi = 3.1$ GeV and $\mathrm{K}_t = 6$ GeV) hardly changes the x range. The leading-twist T-even unpolarized and linearly polarized gluon TMDs can be written as [18,24]

TABLE II. Corresponding values for replica 11.

Parameter	Replica 11	Parameter	Replica 11
A	6.0	κ_2 (GeV^2)	0.414
a	0.78	σ (GeV)	0.50
b	1.38	Λ_X (GeV)	0.448
C	346	κ_1 (GeV^2)	1.46
D (GeV)	0.548		

$$\begin{aligned}\hat{f}_1^g(x, \mathbf{q}_t^2; M_X) &= -\frac{1}{2} g^{ij}[\Phi^{ij}(x, \mathbf{q}_t, S) + \Phi^{ij}(x, \mathbf{q}_t, -S)] \\ &= [(2Mxg_1 - x(M + M_X)g_2)^2[(M_X - M(1-x))^2 + \mathbf{q}_t^2] \\ &\quad + 2\mathbf{q}_t^2(\mathbf{q}_t^2 + xM_X^2)g_2^2 + 2\mathbf{q}_t^2 M^2(1-x)(4g_1^2 - xg_2^2)][(2\pi)^3 4xM^2(L_X^2(0) + \mathbf{q}_t^2)^2]^{-1}, \end{aligned} \tag{71}$$

$$\begin{aligned}\hat{h}_1^{\perp g}(x, \mathbf{q}_t^2; M_X) &= \frac{M^2}{\varepsilon_t^{ij}\delta^{jm}(p_t^j p_t^m + g^{jm}\mathbf{q}_t^2)} \varepsilon_t^{ln}\delta^{nr}[\Phi^{nr}(x, \mathbf{q}_t, S) + \Phi^{nr}(x, \mathbf{q}_t, -S)] \\ &= [4M^2(1-x)g_1^2 + (L_X^2(0) + \mathbf{q}_t^2)g_2^2] \times [(2\pi)^3 x(L_X^2(0) + \mathbf{q}_t^2)^2]^{-1}. \end{aligned} \tag{72}$$

Here, $g_{1,2}(p^2)$ are model-dependent form factors and can be written as

$$g_{1,2}(p^2) = \kappa_{1,2}\frac{p^2}{|p^2 - \Lambda_X^2|^2} = \kappa_{1,2}\frac{p^2(1-x)^2}{(\mathbf{q}_t^2 + L_X^2(\Lambda_X^2))^2}, \tag{73}$$

where $\kappa_{1,2}$ and Λ_X are normalization and cutoff parameters, respectively, and

$$p^2 = -\frac{\mathbf{q}_t^2 + L_X^2(0)}{1-x}, \tag{74}$$

where p is the gluon momentum and

$$L_X^2(\Lambda_X^2) = xM_X^2 + (1-x)\Lambda_X^2 - x(1-x)M^2. \tag{75}$$

The form factors given above are dipolar in nature; the main advantage of using dipolar form factors consists in the possibility of canceling gluon-propagator singularities, quenching the effects of large transverse momenta where a pure TMD description is not any more adequate, and removing logarithmic divergences emerging in p_t-integrated densities.

V. GAUSSIAN PARAMETRIZATION OF THE TMDs

The most widely used parametrizations of the TMDs are Gaussian in nature. Here, both the TMDs f_1^g and $h_1^{\perp g}$ are assumed to be factorized into a product of an x-dependent part given in terms of the collinear PDFs and an exponential factor which is a function of only the transverse momentum ($\mathbf{q}_t$). The width of the Gaussian is usually expressed in terms of the average value of the transverse momentum, which is taken as a model parameter [36–38]:

$$f_1^g(x, \mathbf{q}_t^2) = f_1^g(x, \mu)\frac{1}{\pi\langle\mathbf{q}_t^2\rangle} e^{-\mathbf{q}_t^2/\langle\mathbf{q}_t^2\rangle}, \tag{76}$$

$$h_1^{\perp g}(x, \mathbf{q}_t^2) = \frac{M_p^2 f_1^g(x, \mu)}{\pi\langle\mathbf{q}_t^2\rangle^2}\frac{2(1-r)}{r} e^{1 - \frac{\mathbf{q}_t^2}{r\langle\mathbf{q}_t^2\rangle}}, \tag{77}$$

where $r(0 < r < 1)$ is a parameter and in our case we take $r = 1/3$. The term $f_1^g(x, \mu)$ is the collinear PDF which follows the DGLAP evolution equation. The Gaussian width here is $\langle\mathbf{q}_t^2\rangle = 0.25$ GeV^2. The linearly polarized

gluon distribution in the parametrization above satisfies the positivity bound [18], but does not saturate it:

$$\frac{\mathbf{q}_t^2}{2M_p^2}|h_1^{\perp g}(x,\mathbf{q}_t^2)| \le f_1^g(x,\mathbf{q}_t^2). \tag{78}$$

VI. RESULTS AND DISCUSSION

In the present work, we have numerically calculated the $\cos 2\phi_t$ azimuthal asymmetry in the unpolarized electroproduction of the J/ψ process: $ep \to eJ/\psi$ jet X, within a TMD factorization approach. As depicted in Fig. 2, we have J/ψ and jet almost back to back in the transverse plane as we consider the kinematics $|\mathbf{q}_t| \ll |\mathbf{K}_t|$, which is the required condition to assume TMD factorization. Contributions from the virtual photon-quark (antiquark) initiated subprocesses in the unpolarized cross section is very small in the kinematics considered [42] as compared with the gluon initiated subprocess: $\gamma^* + g \to J/\psi + g$. Therefore, in the numerical estimate of the asymmetry, we have included only the gluon-photon fusion subprocess and neglected the contribution from the quark (antiquark) initiated subprocesses. We have used the MSTW2008 [70] set of collinear PDFs and adopted two sets of LDMEs for the study of azimuthal asymmetry as listed in Table I with the charm mass $m_c = 1.3$ GeV. We used a NRQCD framework for the J/ψ production rate and included contributions from both color singlet and color octet states in the asymmetry. We also calculated the asymmetry taking into consideration contribution only from the CS and compared it with the full NRQCD result incorporating both CS and CO contributions (NRQCD). The contraction of the different states, i.e., ${}^1S_0^{(8)}$, ${}^3S_1^{(1,8)}$, and ${}^3P_{J(=0,1,2)}^{(8)}$, is calculated using FeynCalc [71,72]. We have investigated the effect of TMD evolution on the asymmetry. For the gluon TMDs, we use two parametrizations, Gaussian and based on the spectator model, as discussed above. The J/ψ mass is taken to be $M_\psi = 3.1$ GeV. The collinear PDFs are evaluated at the scale $Q = \sqrt{M_\psi^2 + \mathrm{K}_t^2}$. The numerical results are presented in the kinematical region that can be accessed at the future EIC.

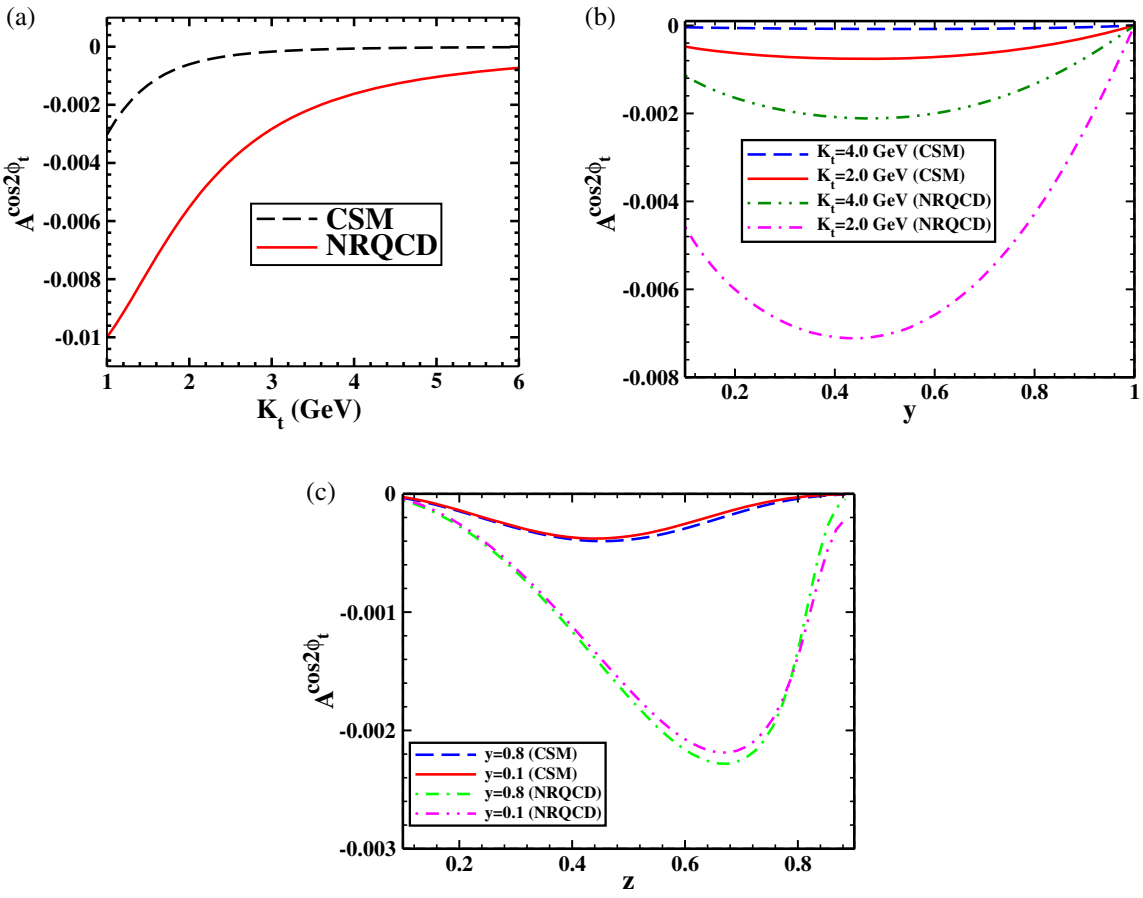

FIG. 3. $\cos 2\phi_t$ asymmetry calculated in TMD evolution approach for $e + p \to e + J/\psi +$ jet $+ X$, in both NRQCD and in the CS; as functions of (a) K_t, (b) y, and (c) z. We have used $\sqrt{s} = 140$ GeV. In (a) and (b), we have used $z = 0.7$. In (a), we have taken $0.1 \le y \le 1$ for the range of y integration, and in (b), we have used fixed values of K_t. In (c), we have taken $\mathrm{K}_t = 3$ GeV and fixed values of y. We have used the Chao-Ma-Shao-Wang-Zhang (CMSWZ) set of LDMEs [55].

We have imposed a cut on the variable z, namely, $0.1 < z < 0.9$, to estimate the asymmetry. As $z \to 1$, the final state gluon becomes soft, which leads to infrared divergences. We impose the upper cut to avoid this gluon becoming soft. The contribution of J/ψ production from fragmentation of the final hard gluon comes from the lower z region, and we impose the lower cut to minimize this contribution. The asymmetry gets maximized around $z = 0.7$ for the kinematics we have considered. Hence, we took $z = 0.7$ for all plots where z is fixed. In addition, we also show the $\cos 2\phi_t$ asymmetry as a function of z. In our estimate, we have neglected the contribution of J/ψ production via feed-down from excited $\psi(2S)$ and the decays of χ_c states.

In Figs. 3–5, we show a comparison of the $\cos 2\phi_t$ azimuthal asymmetry using three different models or parametrizations of the gluon TMDs. Later, in Fig. 7, we have compared them with the asymmetry calculated by satisfying the upper bound of the TMDs [Eq. (78)]. In all plots, we have shown the results when only the CS contributions are included (CS), as well as when both CS and CO contributions are included in NRQCD (NRQCD).

In Fig. 3, we plot the $\cos 2\phi_t$ azimuthal asymmetry in the TMD evolution approach as a function of K_t, y, and z at the center of mass energy $\sqrt{s} = 140$ GeV. The integration ranges are $q_t \in [0.0 - 1.0]$ and $y \in [0.1 - 1.0]$. The range of q_t is considered to satisfy the condition $|\mathbf{q}_t| \ll |\mathbf{K}_t|$. A similar set of plots is shown for the spectator model and for the Gaussian parametrization of the gluon TMDs in Figs. 4 and 5, respectively. In all these plots, we see that, in contrast to the CS case, the NRQCD framework gives a significant contribution to $\cos 2\phi_t$ azimuthal asymmetry at $\sqrt{s} = 140$ GeV. The magnitude of the asymmetry does not change that much if we take a somewhat lower value of $\sqrt{s}$, for example, $\sqrt{s} = 65$ GeV.

In the upper left panel (a) in Figs. 3–5, we have plotted the $\cos 2\phi_t$ asymmetry as functions of K_t at $\sqrt{s} = 140$ GeV. In these plots, we integrated q_t and y in the range (0,1) and (0.1,1), respectively. We see that the $\cos 2\phi_t$ asymmetry is maximum (negative) for lower K_t and monotonically

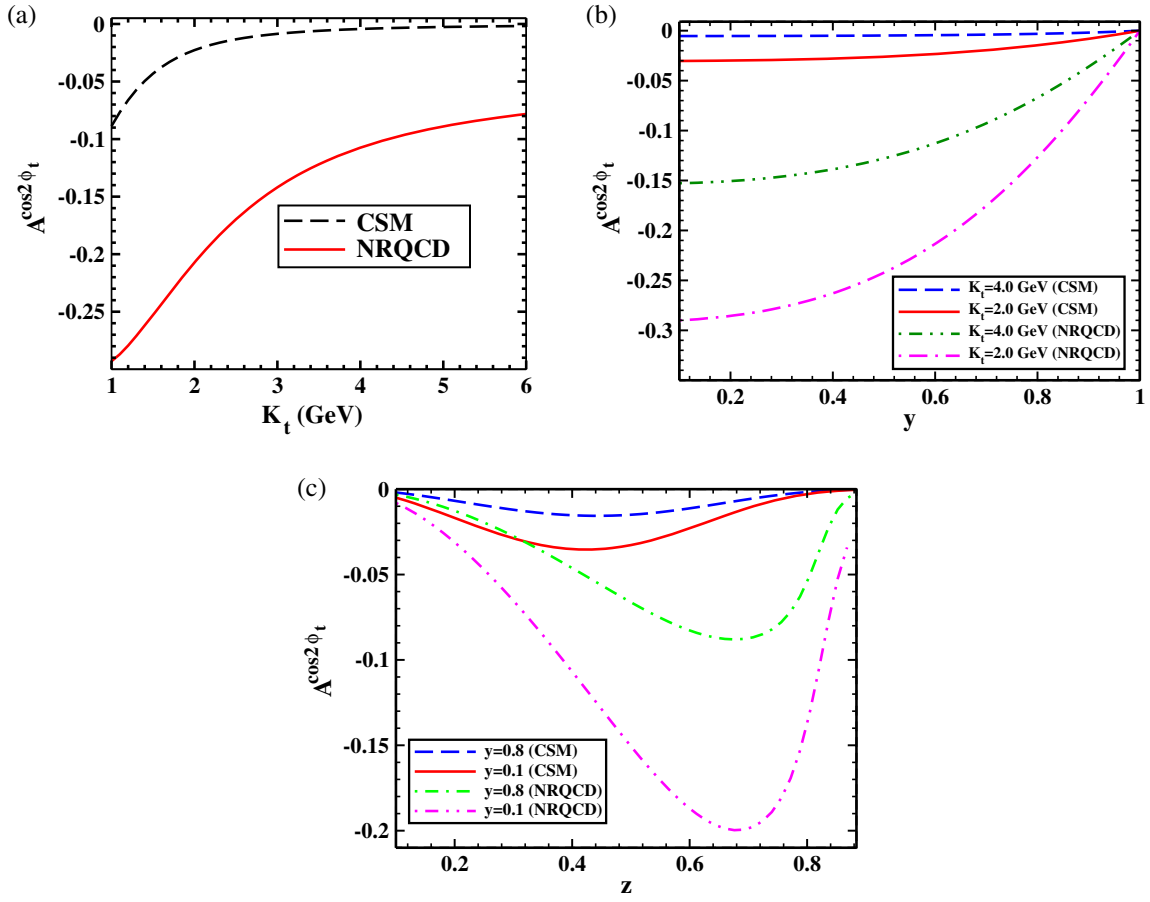

FIG. 4. $\cos 2\phi_t$ asymmetry calculated in the spectator model for the $e + p \to e + J/\psi + \text{jet} + X$ process, in both NRQCD and in the CS; as functions of (a) K_t, (b) y, and (c) z. We have used $\sqrt{s} = 140$ GeV. In (a) and (b), we have used $z = 0.7$. In (a), we have taken $0.1 \le y \le 1$ for the range of y integration, and in (b), we have used fixed values of K_t. In (c), we have taken $K_t = 3$ GeV and fixed values of y. We have used the CMSWZ set of LDMEs [55].

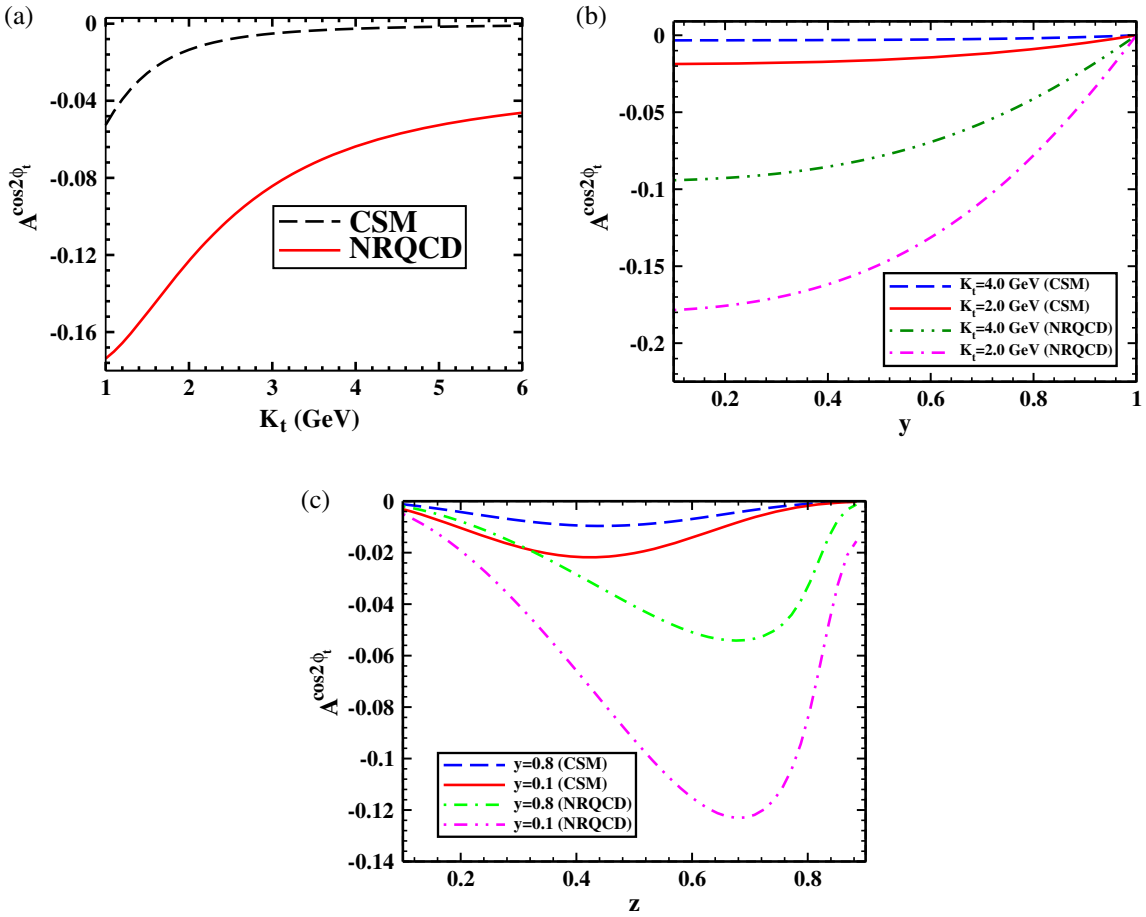

FIG. 5. $\cos 2\phi_t$ asymmetry calculated using Gaussian parametrization of TMDs for the $e + p \to e + J/\psi + \text{jet} + X$ process, as functions of (a) K_t, (b) y, and (c) z. We have used $\sqrt{s} = 140$ GeV. In (a) and (b), we have used $z = 0.7$. In (a), we have taken $0.1 \le y \le 1$ for the range of y integration, and in (b), we have used fixed values of K_t. In (c), we have taken $K_t = 3$ GeV and fixed values of y. We have used the CMSWZ set of LDMEs [55].

decreases as we go in the higher K_t region. The maximum asymmetry we obtained is ≈29% in the spectator model at $K_t = 1$ GeV followed by the Gaussian parametrization, ≈17%. Incorporation of the TMD evolution results in a smaller asymmetry, ≈1% at $K_t = 1$ GeV.

The y dependence of $\cos 2\phi_t$ azimuthal asymmetry is shown in the upper right panel (b) in Figs. 3–5 at $\sqrt{s} = 140$ GeV; we have shown the results both in NRQCD and in the CS. We plotted the asymmetry for two fixed values of K_t, namely, 2 and 4 GeV. We have plotted the asymmetry in the range of $y \in [0.1, 1]$; however, in the lower y region, the magnitude of the asymmetry is similar in both the spectator and the Gaussian models, whereas in the TMD evolution approach, the asymmetry is maximum around $y = 0.44$ at $K_t = 2$ GeV in NRQCD. The asymmetry is small in the TMD evolution approach; however, we obtain a significant asymmetry, ≈29%, in the spectator model followed with ≈18% in the Gaussian model at $K_t = 2$ GeV and $y = 0.1$.

In all the above discussed plots of the asymmetry as functions of K_t and y, we have taken a fixed value of $z = 0.7$. However, in the lower panel (c) in Figs. 3–5, we have plotted the $\cos(2\phi_t)$ asymmetry as functions of z at $\sqrt{s} = 140$ GeV and $K_t = 3$ GeV for both NRQCD and the CS. We have taken fixed values of y, namely, 0.1 and 0.8. The peak of the asymmetry is ≈12% at $z \approx 0.7$ in NRQCD and ≈2% at $z \approx 0.4$ in the CS at $y = 0.1$. In all these plots, we have used LDMEs from Ref. [55].

In Fig. 6, we have plotted both the TMDs f_1^g and $h_1^{\perp g}$ and their ratio $\frac{q_t^2 h_1^{\perp g}}{2M_P^2 f_1^g}$ as functions of q_t for all three parametrizations. In all these plots, we have used similar kinematics as we considered for the plots in Figs. 3–7. In this kinematics, the x values of the gluon TMDs are of the order of 10^{-3}–10^{-2}. We have plotted at the probing scale, which is the virtuality of photon, $Q^2 = M_\psi^2 + K_t^2$, where $K_t = 3$ GeV and at the fixed values of $y = 0.3$ and $z = 0.7$. This sets $x \approx 0.012$. From the plots of the ratio $\frac{q_t^2 h_1^{\perp g}}{2M_P f_1^g}$ [Fig. 6(d)], we see that the TMDs in the spectator model indeed saturate the positivity bound, whereas the Gaussian parametrizations and TMD evolution approach

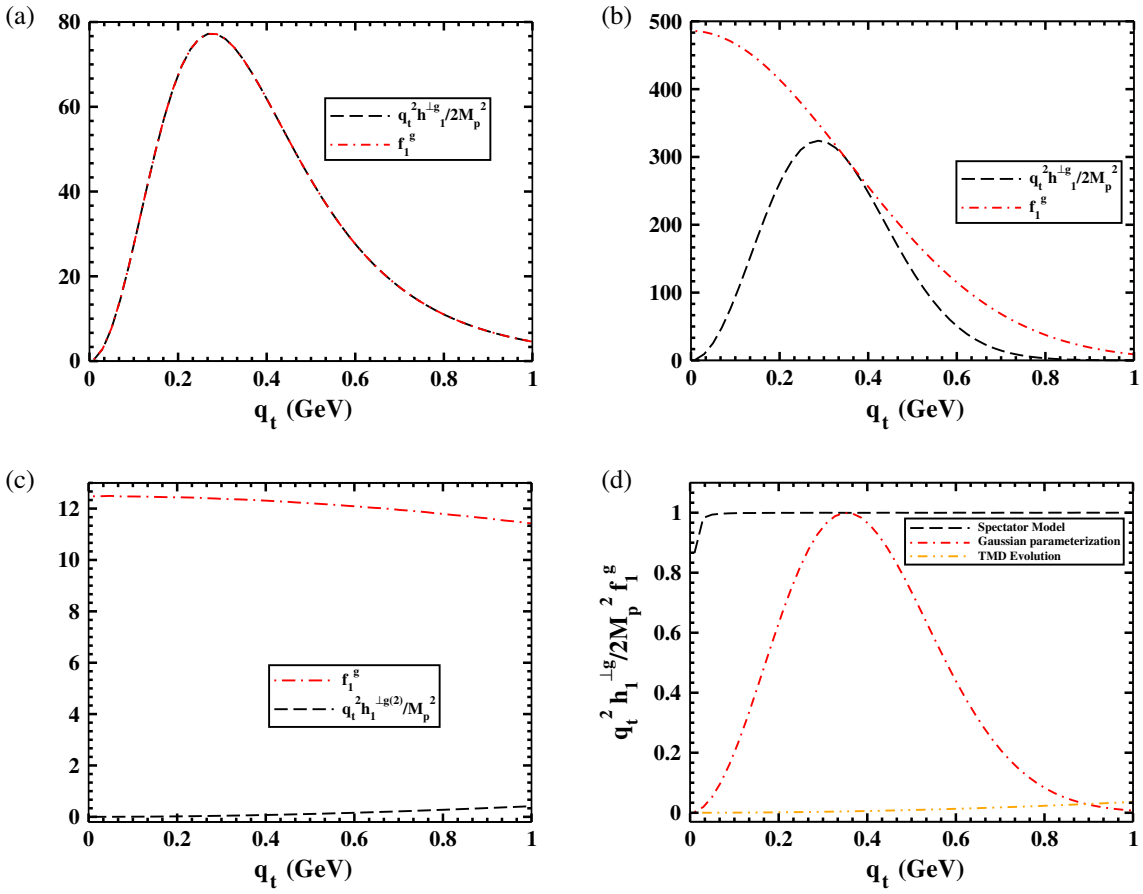

FIG. 6. Unpolarized and linearly polarized gluon TMDs as a function of q_t calculated in the spectator model (a), Gaussian model (b), and TMD evolution (c), respectively, at $\sqrt{s} = 140$, $K_t = 3.0$ GeV, $y = 0.3$, and $z = 0.7$. (d) shows the comparison between the positivity bound for all the parametrizations.

satisfy the positivity bound but do not saturate it except for $q_t \approx 0.36$ GeV, where Gaussian parametrization is saturating the positivity bound. Moreover, the ratio is larger in the case of the Gaussian as compared with the TMD evolution approach for almost the whole range of q_t considered. In the spectator model, tails of the TMDs in the small-x domain depend on the trend of spectral function at large M_X [69]. We have checked that the spectator model results in Eqs. (12) and (15) in Ref. [69] for the ratio $\frac{q_t^2 h_1^{\perp g}}{2M_P^2 f_1^g}$ at $x = 0.001$ without integrating over the spectral function and does not saturate the positivity bound when M_X is large. However, if we multiply by the spectral function and integrate over M_X, the TMDs saturate the positivity bound when x is of the order of 10^{-3}–10^{-2}; this could be because the spectral function is zero for higher values of M_X in replica 11. However, in the higher x region, the TMDs do not saturate the bound but satisfy it for the whole range of the transverse momentum, q_t.

In Fig. 7, we show a comparison of the upper bound of the asymmetry with that calculated in spectator model, Gaussian model, and TMD evolution approach at $\sqrt{s} = 140$ GeV. The upper bound of the asymmetry is calculated by saturating the positivity bound of TMDs in Eq. (78) and fixing all the parameters mentioned above. We have shown the result in both NRQCD and CS as a function of K_t at $y = 0.3$ (upper panel) and as a function of y at $K_t = 2$ GeV in the lower panel. In the case of TMD evolution, the nonperturbative Sudakov factor corresponds to $b_{t\,\mathrm{lim}} = 2$ GeV^{-1}. For all the plots the range of integration of $q_t \in [0.0\text{–}1.0]$ GeV, $z = 0.7$ and we have fixed the virtuality of photon $Q = \sqrt{M_\psi^2 + K_t^2}$.

We can see that the asymmetry calculated with the spectator model is maximum and agrees with the upper bound. As seen from Fig. 7, the asymmetry incorporating TMD evolution is significantly smaller than that calculated using Gaussian and spectator models for the gluon TMDs. This is because the denominator of the asymmetry receives contribution from the unpolarized gluon distribution which has a LO term Eq. (61), whereas the numerator contains the linearly polarized gluon distribution whose leading contribution comes at $O(\alpha_s)$. If we exclude the LO term in the unpolarized gluon TMD, we find the asymmetry increases approximately 3 times. We also find that the magnitude of the asymmetry does not change much if $\sqrt{s}$ is lower.

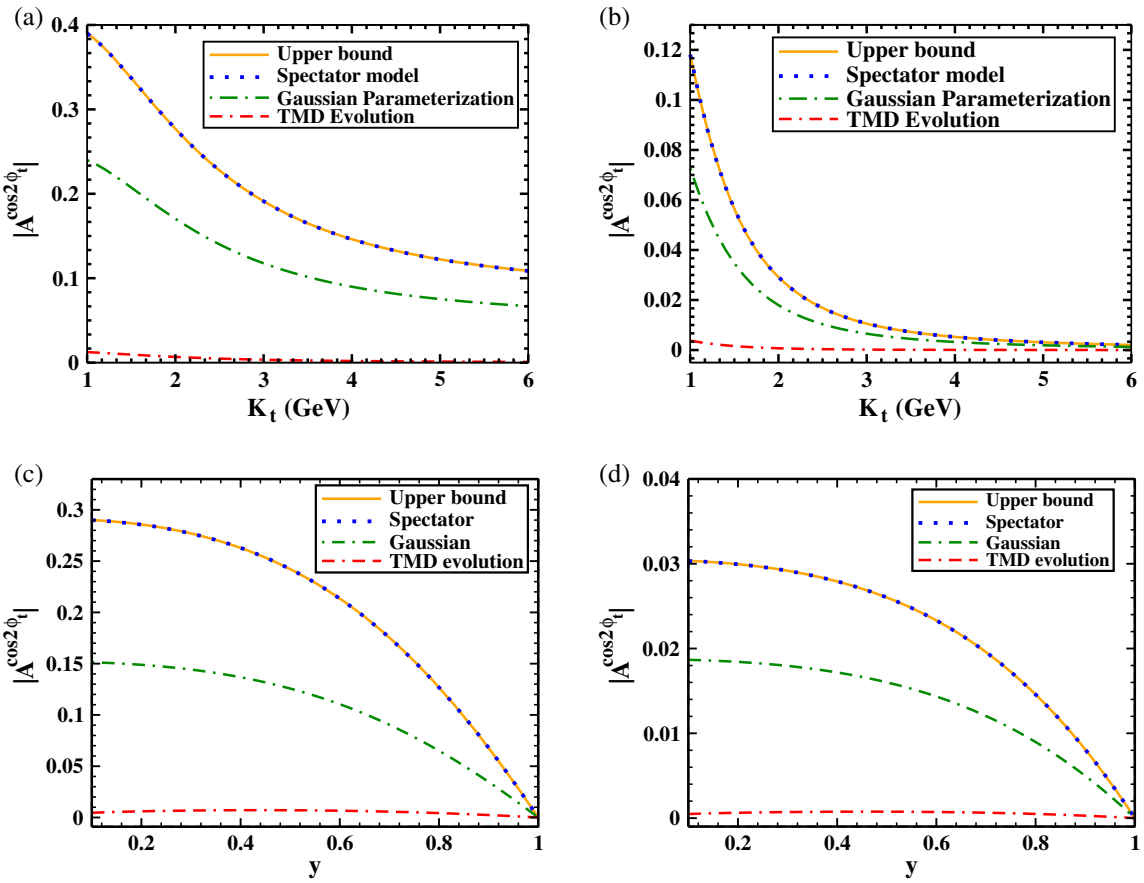

FIG. 7. Upper bound of the asymmetry compared with the absolute values of $A^{\cos 2\phi_t}$ calculated in the spectator model, Gaussian model, and TMD evolution, respectively, for $e^- + P \to e^- + J/\psi + \text{jet} + X$ at $\sqrt{s} = 140$. The left panel shows the asymmetry in NRQCD and the right panel in CS. We have taken $y = 0.3$ in the upper panels [(a) and (b)] and $K_t = 2$ GeV in the lower panels [(c) and (d)].

Lastly, in Fig. 8, we show the upper bound for the absolute value of $|A^{\cos 2\phi_t}|$ within the NRQCD using two sets of LDMEs, as well as the contributions coming from individual states, i.e., ${}^1S_0^{(8)}$, ${}^3S_1^{(1,8)}$, and ${}^3P_j^{(8)}$. One can see from Fig. 8(a) that, for the LDME set CMSWZ [55], the dominating contribution comes from one single state, ${}^1S_0^{(8)}$; while from Fig. 8(b) one can see that, for the Sharma-Vitev (SV) set of LDME [54], the dominating contribution comes

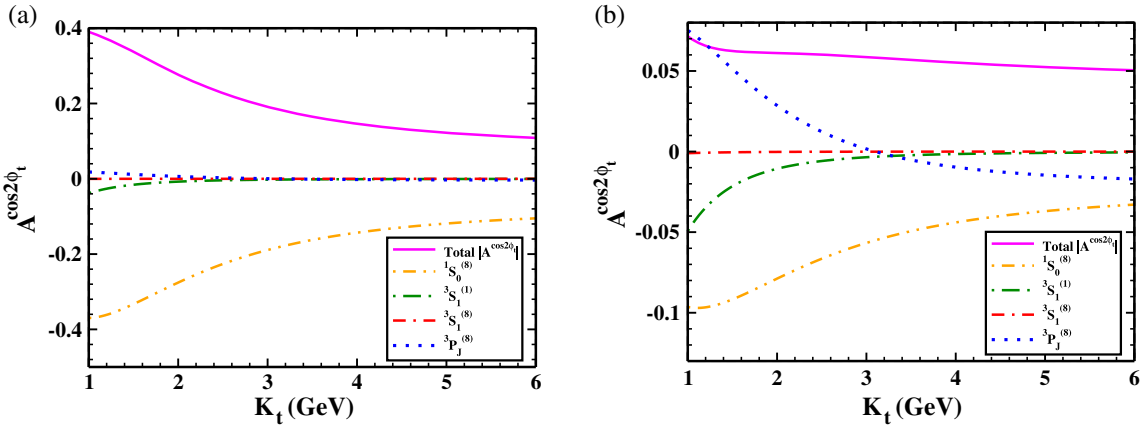

FIG. 8. Contribution to the upper bound of the asymmetry coming from individual states, as a function of K_t at $\sqrt{s} = 140$ GeV, $Q = \sqrt{M_\psi^2 + K_t^2}$, and $y = 0.3$, (a) using the CMSWZ set of LDMEs [55] and (b) using the SV set of LDMEs [54].

from two states, ${}^1S_0^{(8)}$ and ${}^3P_j^{(8)}$. So, we can conclude that the asymmetry depends on the LDME set chosen. It is worth mentioning here that our results for the upper bound of the asymmetry do not match with those presented in Ref. [42] even if we plot it using the same scale as in this reference. We have traced this mismatch to a difference in the sign of the contribution coming from the ${}^3P_0^{(8)}$ state to the coefficient $\mathbb{B}_0$.

VII. CONCLUSION

We have presented a calculation of the $\cos 2\phi_t$ asymmetry in almost back-to-back production of a J/ψ and a jet in ep collision, using TMD factorization and a generalized parton model. This asymmetry is sensitive to the still-unknown linearly polarized gluon distribution. We present a numerical estimate of the asymmetry in the kinematical region that will be accessible at the future EIC. We have used NRQCD to calculate the J/ψ production rate and two recent parametrizations for the gluon TMDs, one based on a Gaussian-type distribution and another based on a spectator model. The asymmetry is quite sizable; in fact, in the spectator model, the asymmetry agrees with the upper bound that is obtained by saturating the positivity condition of the gluon TMDs. TMD evolution affects the asymmetry at the energy of the EIC, making it smaller. The asymmetry also depends on the LDMEs used, and the dominating contribution comes from different states. We conclude that the back-to-back production of J/ψ and a jet at the future EIC will be a very useful channel to probe the linearly polarized gluon TMDs.

ACKNOWLEDGMENTS

We acknowledge the funding from Board of Research in Nuclear Sciences (BRNS), Government of India, under sanction No. 57/14/04/2021-BRNS/57082. We thank A. Bacchetta, M. Radici, and F. Celiberto for useful discussion.

[1] P. J. Mulders and R. D. Tangerman, Nucl. Phys. **B461**, 197 (1996); **B484**, 538(E) (1997).
[2] D. Boer and P. Mulders, Phys. Rev. D **57**, 5780 (1998).
[3] D. Boer, R. Jakob, and P. Mulders, Nucl. Phys. **B564**, 471 (2000).
[4] M. Anselmino, M. Boglione, and F. Murgia, Phys. Rev. D **60**, 054027 (1999).
[5] M. Anselmino, M. Boglione, and F. Murgia, Phys. Lett. B **362**, 164 (1995).
[6] V. Barone, A. Drago, and P. G. Ratcliffe, Phys. Rep. **359**, 1 (2002).
[7] J. Collins, *Foundations of Perturbative QCD* (Cambridge University Press, Cambridge, England, 2011), Vol. 32.
[8] M. G. Echevarria, A. Idilbi, and I. Scimemi, J. High Energy Phys. 07 (2012) 002.
[9] M. G. Echevarría, A. Idilbi, and I. Scimemi, Phys. Lett. B **726**, 795 (2013).
[10] M. G. Echevarria, J. High Energy Phys. 10 (2019) 144.
[11] A. Bacchetta, D. Boer, M. Diehl, and P. J. Mulders, J. High Energy Phys. 08 (2008) 023.
[12] S. Fleming, Y. Makris, and T. Mehen, J. High Energy Phys. 04 (2020) 122.
[13] J. C. Collins, Phys. Lett. B **536**, 43 (2002).
[14] X. Ji and F. Yuan, Phys. Lett. B **543**, 66 (2002).
[15] A. V. Belitsky, X. Ji, and F. Yuan, Nucl. Phys. **B656**, 165 (2003).
[16] D. Boer, P. Mulders, and F. Pijlman, Nucl. Phys. **B667**, 201 (2003).
[17] M. Anselmino, M. Boglione, U. D'Alesio, F. Murgia, and A. Prokudin, J. High Energy Phys. 04 (2017) 046.
[18] P. Mulders and J. Rodrigues, Phys. Rev. D **63**, 094021 (2001).
[19] J.-P. Lansberg, C. Pisano, F. Scarpa, and M. Schlegel, Phys. Lett. B **784**, 217 (2018).
[20] M. Buffing, A. Mukherjee, and P. Mulders, Phys. Rev. D **88**, 054027 (2013).
[21] Y. V. Kovchegov and A. H. Mueller, Nucl. Phys. **B529**, 451 (1998).
[22] L. McLerran and R. Venugopalan, Phys. Rev. D **59**, 094002 (1999).
[23] F. Dominguez, J.-W. Qiu, B.-W. Xiao, and F. Yuan, Phys. Rev. D **85**, 045003 (2012).
[24] S. Meissner, A. Metz, and K. Goeke, Phys. Rev. D **76**, 034002 (2007).
[25] C. Marquet, C. Roiesnel, and P. Taels, Phys. Rev. D **97**, 014004 (2018).
[26] C. Pisano, D. Boer, S. J. Brodsky, M. G. A. Buffing, and P. J. Mulders, J. High Energy Phys. 10 (2013) 024.
[27] D. Boer, P. J. Mulders, and C. Pisano, Phys. Rev. D **80**, 094017 (2009).
[28] A. Efremov, N. Y. Ivanov, and O. Teryaev, Phys. Lett. B **777**, 435 (2018).
[29] A. Efremov, N. Y. Ivanov, and O. Teryaev, Phys. Lett. B **780**, 303 (2018).
[30] J.-P. Lansberg, C. Pisano, and M. Schlegel, Nucl. Phys. **B920**, 192 (2017).
[31] A. Dumitru, V. Skokov, and T. Ullrich, Phys. Rev. C **99**, 015204 (2019).
[32] P. Sun, B.-W. Xiao, and F. Yuan, Phys. Rev. D **84**, 094005 (2011).
[33] D. Boer, W. J. Den Dunnen, C. Pisano, and M. Schlegel, Phys. Rev. Lett. **111**, 032002 (2013).
[34] D. Boer, W. J. den Dunnen, C. Pisano, M. Schlegel, and W. Vogelsang, Phys. Rev. Lett. **108**, 032002 (2012).

[35] M. G. Echevarria, T. Kasemets, P. J. Mulders, and C. Pisano, J. High Energy Phys. 07 (2015) 158; 05 (2017) 073(E).
[36] D. Boer and C. Pisano, Phys. Rev. D **86**, 094007 (2012).
[37] A. Mukherjee and S. Rajesh, Phys. Rev. D **95**, 034039 (2017).
[38] A. Mukherjee and S. Rajesh, Phys. Rev. D **93**, 054018 (2016).
[39] S. Rajesh, U. D'Alesio, A. Mukherjee, F. Murgia, and C. Pisano, arXiv:2108.04866.
[40] A. Mukherjee and S. Rajesh, Eur. Phys. J. C **77**, 854 (2017).
[41] R. Kishore and A. Mukherjee, Phys. Rev. D **99**, 054012 (2019).
[42] U. D'Alesio, F. Murgia, C. Pisano, and P. Taels, Phys. Rev. D **100**, 094016 (2019).
[43] R. Kishore, A. Mukherjee, and S. Rajesh, Phys. Rev. D **101**, 054003 (2020).
[44] P. Hägler, R. Kirschner, A. Schäfer, L. Szymanowski, and O. Teryaev, Phys. Rev. Lett. **86**, 1446 (2001).
[45] F. Yuan and K.-T. Chao, Phys. Rev. Lett. **87**, 022002 (2001).
[46] F. Yuan, Phys. Rev. D **78**, 014024 (2008).
[47] G. T. Bodwin, E. Braaten, and G. P. Lepage, Phys. Rev. D **51**, 1125 (1995); **55**, 5853(E) (1997).
[48] D. Boer, C. Pisano, and P. Taels, Phys. Rev. D **103**, 074012 (2021).
[49] G. P. Lepage, L. Magnea, C. Nakhleh, U. Magnea, and K. Hornbostel, Phys. Rev. D **46**, 4052 (1992).
[50] E. L. Berger and D. Jones, Phys. Rev. D **23**, 1521 (1981).
[51] R. Baier and R. Rückl, Z. Phys. C **19**, 251 (1983).
[52] S. Rajesh, R. Kishore, and A. Mukherjee, Phys. Rev. D **98**, 014007 (2018).
[53] D. Boer and C. Pisano, Phys. Rev. D **86**, 094007 (2012).
[54] R. Sharma and I. Vitev, Phys. Rev. C **87**, 044905 (2013).
[55] K.-T. Chao, Y.-Q. Ma, H.-S. Shao, K. Wang, and Y.-J. Zhang, Phys. Rev. Lett. **108**, 242004 (2012).
[56] D. Graudenz, Phys. Rev. D **49**, 3291 (1994).
[57] S. M. Aybat and T. C. Rogers, Phys. Rev. D **83**, 114042 (2011).
[58] S. M. Aybat, A. Prokudin, and T. C. Rogers, Phys. Rev. Lett. **108**, 242003 (2012).
[59] M. G. Echevarria, A. Idilbi, Z.-B. Kang, and I. Vitev, Phys. Rev. D **89**, 074013 (2014).
[60] S. M. Aybat, J. C. Collins, J.-W. Qiu, and T. C. Rogers, Phys. Rev. D **85**, 034043 (2012).
[61] M. G. Echevarria, A. Idilbi, and I. Scimemi, Phys. Rev. D **90**, 014003 (2014).
[62] D. Boer, U. D'Alesio, F. Murgia, C. Pisano, and P. Taels, 09 J. High Energy Phys. (2020) 40.
[63] R. Tangerman and P. Mulders, Phys. Rev. D **51**, 3357 (1995).
[64] T. van Daal, arXiv:1612.06585.
[65] Y. V. Kovchegov and E. Levin, *Quantum Chromodynamics at High Energy* (Cambridge University Press, Cambridge, England, 2012).
[66] F. Scarpa, D. Boer, M. G. Echevarria, J.-P. Lansberg, C. Pisano, and M. Schlegel, Eur. Phys. J. C **80**, 87 (2020).
[67] F. Landry, R. Brock, P. M. Nadolsky, and C.-P. Yuan, Phys. Rev. D **67**, 073016 (2003).
[68] S. M. Aybat and T. C. Rogers, Phys. Rev. D **83**, 114042 (2011).
[69] A. Bacchetta, F. G. Celiberto, M. Radici, and P. Taels, Eur. Phys. J. C **80**, 733 (2020).
[70] A. D. Martin, W. J. Stirling, R. S. Thorne, and G. Watt, Eur. Phys. J. C **63**, 189 (2009).
[71] V. Shtabovenko, R. Mertig, and F. Orellana, Comput. Phys. Commun. **256**, 107478 (2020).
[72] R. Mertig, M. Böhm, and A. Denner, Comput. Phys. Commun. **64**, 345 (1991).